Underground hydrogen storage: A critical assessment of fluid-fluid and fluid-rock interactions

Underground hydrogen storage: A critical assessment of fluid-fluid and fluid-rock interactions

Afeez O. Gbadamosi[1], Nasiru S. Muhammed[1], Shirish Patil[1*], Dhafer Al Shehri[1], Bashirul Haq[1], Emmanuel I. Epelle[2,3], Mohamed Mahmoud[1], Muhammad Shahzad Kamal[4*]

[1] Department of Petroleum Engineering, College of Petroleum Engineering and Geosciences, King Fahd University of Petroleum and Minerals, Dhahran, 31261, Saudi Arabia.

[2] School of Computing, Engineering & Physical Sciences, University of the West of Scotland, Paisley, PA1 2BE, United Kingdom

[3] School of Engineering, Institute for Materials and Processes, The University of Edinburgh, Sanderson Building, Robert Stevenson Road, Edinburgh, EH9 3FB, United Kingdom

[4] Center for Integrative Petroleum Research (CIPR), College of Petroleum Engineering and Geosciences, King Fahd University of Petroleum and Minerals, Dhahran 31261, Saudi Arabia.

*Corresponding Email: patil@kfupm.edu.sa

shahzadmalik@kfupm.edu.sa

Abstract

Underground hydrogen storage (UHS) is the injection of hydrogen into the geologic porous medium for subsequent withdrawal and reuse during off-peak periods to contribute to the energy mix. Recently, UHS has gained prodigious attention due to its efficiency for the storage of hydrogen on a large scale. Nonetheless, an adequate understanding of the storage process is required for efficient and safe monitoring and to preserve reservoir integrity. Herein, the hydrodynamics of injected hydrogen (H_2) gas, reservoir fluids, and reservoir rock systems are reviewed. Moreover, critical factors inherent to the reservoir (such as temperature, pressure, salinity, and rock mineralogy) that affect the UHS process are elucidated. Based on the available literature, the interplay of H_2 solubility, interfacial tension, wettability, adsorption, and diffusion properties influence the geologic storage process. Overall, this review provides extensive insight into fluid-fluid and fluid-rock interactions and their effect on underground hydrogen storage process. Future research should focus on optimizing the process parameters to improve storage and withdrawal efficiency, thus guarantee energy security.

Keywords: Underground hydrogen storage, interfacial tension, wettability, adsorption, solubility, diffusivity.

1. Introduction

There is a constant increase in global energy demand due to increasing population and global industrialization [1,2]. Currently, a significant contribution to the world's energy demand comes from non-renewable sources like petroleum, and coal [3–5]. The use of fossil fuels for energy is a cause for concern due to post-combustion emissions of carbon monoxide (CO), carbon dioxide (CO_2), and nitrous oxide (NO_2) which constitute greenhouse gas emissions [6,7]. The release of these gases into the atmosphere causes the greenhouse effect and consequently, contributes to global warming and climate change. Intergovernmental policy on recent (IPCC) and several other global organizations are working assiduously to ensure a reduction in emissions to save the planet earth. Consequently, renewable sources such as hydro, geothermal, wind, solar, and hydrogen are receiving enormous attention [8–10].

Of the numerous renewable energies, hydrogen offers the greatest potential based on technoeconomic analyses [11,12]. It has inherent characteristics and unique properties such as light weight, high calorific value, and high gravimetric density. The utilization of hydrogen in the energy mix includes applications such as direct fuel for heat and power, power-to-gas technology, and utilization in fuel cells, aerospace, and metallurgical industries [13–15]. Moreover, hydrogen is also applied for refining and upgrading fossil fuels, and conversion of syngas to value-added products [7,16]. Compared to other sources of renewable energy, they are unaffected by cyclic seasonal changes which may disrupt power generation and usage [17]. To achieve full incorporation of hydrogen energy for global energy supply, concerted efforts are required to ensure suitable and sustainable large-scale storage of hydrogen [18,19]. Hence, hydrogen storage has attracted global interest because it poses the major stumbling block to achieving several targets for hydrogen contribution towards energy generation and utilization [20].

Hydrogen is usually stored in the gaseous or liquid form and several storage methods have been proffered for hydrogen. These can be widely categorized into physical storage methods, material-based storage, and underground hydrogen storage [21]. Physical storage methods involve the compression of hydrogen at extremely low temperatures and high pressures in tanks and cylinders. However, the shortcoming of this method includes high energy consumption, low volumetric capacity, and the requirement of heat management to avoid explosion [22,23].

Contrariwise, material-based storage entails the storage of hydrogen on solid-state materials such as hydrogen clathrates, porous adsorbents, and metal hydrides [24,25]. Nevertheless, the stability, kinetics, and thermodynamics of the process remain challenging.

More recently, underground hydrogen storage has gained prominence due to its efficiency for large-scale storage of hydrogen. Underground hydrogen storage (UHS) offers a low-cost pathway for the storage of hydrogen in a geological medium [26,27]. As compared to other storage techniques that require the use of expensive tanks or materials, UHS offers savings on storage expenses as it can be conducted with modifications of existing facilities used for depleted natural gas fields. The recognized media used for UHS includes coal seams, saline aquifers, and depleted hydrocarbon reservoirs [20,28,29]. Currently, depleted gas reservoir and salt cavern accounts for large percentage of existing UHS projects worldwide. Field applications of UHS have been reported in Clemens (USA), Beynes (France), Diadema (Argentina), and Teesside (United Kingdom) [30,31].

UHS in depleted oil and gas reservoirs offers immense benefits [30,32]. Firstly, they have a confirmed trap structure, caprock, and porous and permeable reservoir formation [33]. Moreover, they have inherent fluids that can act as buffer to improve the H_2 storage process. Nonetheless, the petrophysical properties of the porous medium are complex. With varying porosities, permeabilities, heterogeneities, and rock compositions, the process of injection and withdrawal of hydrogen during UHS requires appropriate screening of the subsurface formations to be utilized such as to minimize and/or eradicate avoidable losses that may occur in such formations. For suitable screening of subsurface formation for UHS, fluid-fluid and fluid-rock interactions are crucial parameters. These parameters govern the sealing capacities of caprock, pore-scale distribution and saturation of H_2 in the pore space, and displacement of fluids as illustrated in **Figure 1**.

Numerous reviews exist in the literature on UHS processes. However, most of the reviews focus on potential storage sites such as salt caverns, and saline aquifers and identifying the challenges associated with UHS [11,20,27,34–36]. Due to the paucity of data, only a handful of review exists on UHS in conventional and unconventional reservoirs. Besides, few of the existing reviews on UHS in depleted oil/gas reservoirs have focussed on the comparative analysis of hydrogen gas (H_2) gas, carbon dioxide (CO_2), methane (CH_4), and Nitrogen (N_2) as pressure-support/cushion gases for UHS applications [10,37]. More recently, due to an upsurge in research on UHS, an avalanche of data has emerged providing more insights into the

hydrodynamics of UHS processes. Herein, an extensive review of UHS in conventional and unconventional reservoirs with adequate consideration of fluid-fluid and fluid-rock interaction is conducted. Firstly, the fluid-fluid properties of solubility and fluid-fluid IFT are discussed. Subsequently, the rock-fluid properties such as rock-fluid IFT, wettability, adsorption, and diffusion behavior of the H_2 gas are elucidated. This work intends to assess and properly elucidate the current state-of-the-art, identify the research gaps, and provide recommendations for future works on UHS.

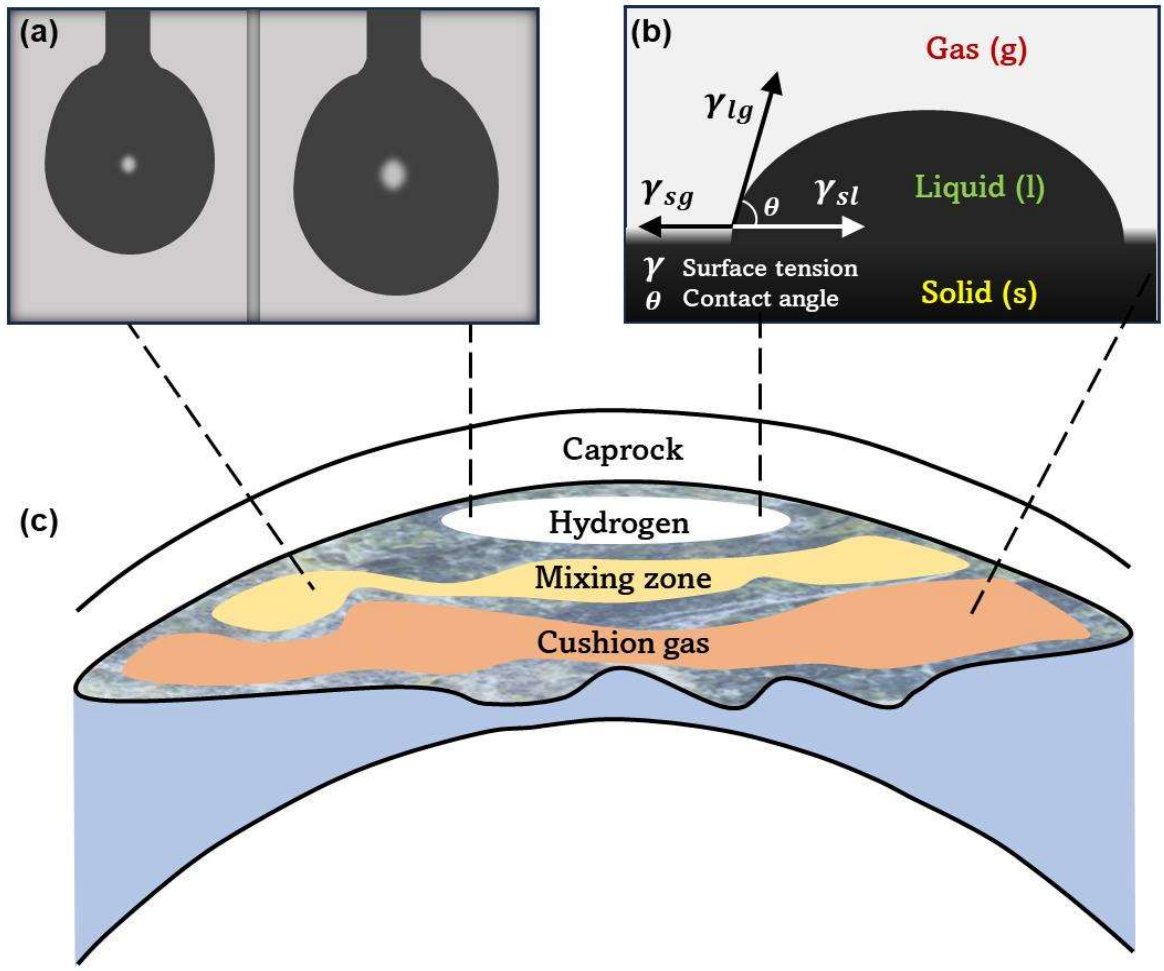

Fig. 1. (a) Fluid-fluid, (b) fluid-rock, and (c) reservoir system interactions during UHS. Modified after [17].

2. Solubility

The concept of solubility is an important factor in determining losses and gas trapping in subsurface formations. For instance, gases are usually contained (or trapped) in the subsurface

via structural, capillary, dissolution (solubility), mineralization, and adsorption mechanisms [10,30].

Structural trapping occurs when gas is trapped within the pores or fractures of the rock formation due to the shape, size, and pore network connectivity. This trapping mechanism is dependent on the properties of the reservoir rock such as permeability, porosity, and pore throat size. Capillary trapping occurs when gas is trapped in the form of small droplets due to capillary forces at the interface between the gas and the liquid phases and is dependent on the properties of the pore fluid such as surface tension and contact angle. Solubility trapping occurs when gas is dissolved in the pore fluid and is prevented from escaping due to the low solubility of the gas in the liquid phase. Mineralization trapping on the other hand occurs when the injected gas interacts with the formation's minerals and fluids. These trapping mechanisms (i.e., dissolution and mineralization) are dependent on the properties of the pore fluid such as salinity, pH, and temperature. Adsorption trapping, however, occurs when gas molecules are adsorbed onto the surface of the mineral grains in the rock formation due to the attractive forces between the gas molecules and the mineral surfaces. This trapping mechanism is dependent on the properties of the mineral surface such as surface area, surface chemistry, and pore size distribution [10,30].

In the case of UHS, trapping mechanisms such as solubility (fluid-fluid – discussed herein) and mineralization (fluid-rock) can lead to the permanent loss of the injected gas, making them unfavorable. For example, if the solubility of a gas is high, more of the injected gas will dissolve into the fluids, which can reduce the amount of gas trapped in the pore spaces. However, if the solubility of gas is low, less of the injected gas will dissolve into the fluids, thus, the amount of gas trapped in the pore space increases (see refs. for three phase IFT study [38]). Therefore, understanding the solubility of hydrogen gas in the reservoir fluids (e.g., brine) in a three-phase region is an important factor that determines how much of the injected gas can be lost via dissolution into the fluids and how much will remain as a separate gas phase.

The experimental data depicted in **Figure 2** reveals that H_2 solubility is dependent on factors such as pressure, temperature, and salinity. However, the solubility characteristics of H_2 differ when it is dissolved in an aqueous solution compared to a non-aqueous solution [39]. This disparity is attributed to the diverse types of fluid compositions present, which will be elaborated upon in the subsequent discussion.

According to literature [40,41], temperature, pressure, and reservoir salinity have a significant impact on H_2 solubility under UHS conditions, as depicted in **Figures 2(a) to (c)**. An increase in pressure and temperature generally results in an increase in H_2 dissolution, while an increase in brine salinity leads to a decrease in H_2 solubility. For example, at 372 K, raising the pressure from 3.3 MPa to 23 MPa increased the H_2 solubility in 3 mol/kg NaCl brine from 2.15×10^{-5} mole fraction to 1.3×10^{-3} mole fraction (refer to **Figure 2(a)**). Similarly, at 10.1 MPa, increasing the temperature from 323 K to 373 K resulted in an increase in H_2 solubility in 3 mol/kg NaCl brine from 6.32×10^{-4} mole fraction to 7.03×10^{-4} mole fraction (see **Figure 2(b)**). Additionally, H_2 solubility slightly decreased from 9.38×10^{-4} mole fraction to 6.62×10^{-4} mole fraction at 15.1 MPa and 323 K as brine salinity increased from 3 mol/kg to 5 mol/kg (see **Figure 2(c)**) [40,41].

The observed trend in **Figure 2** has been reported in various solubility studies, including both experimental and simulation works. Experimental studies have been conducted on H_2-pure water [40–46] and H_2-aqueous solution [41,47,48] systems. On the other hand, simulation studies have focused solely on H_2-aqueous solution systems, as observed in different literature [39,49–51].

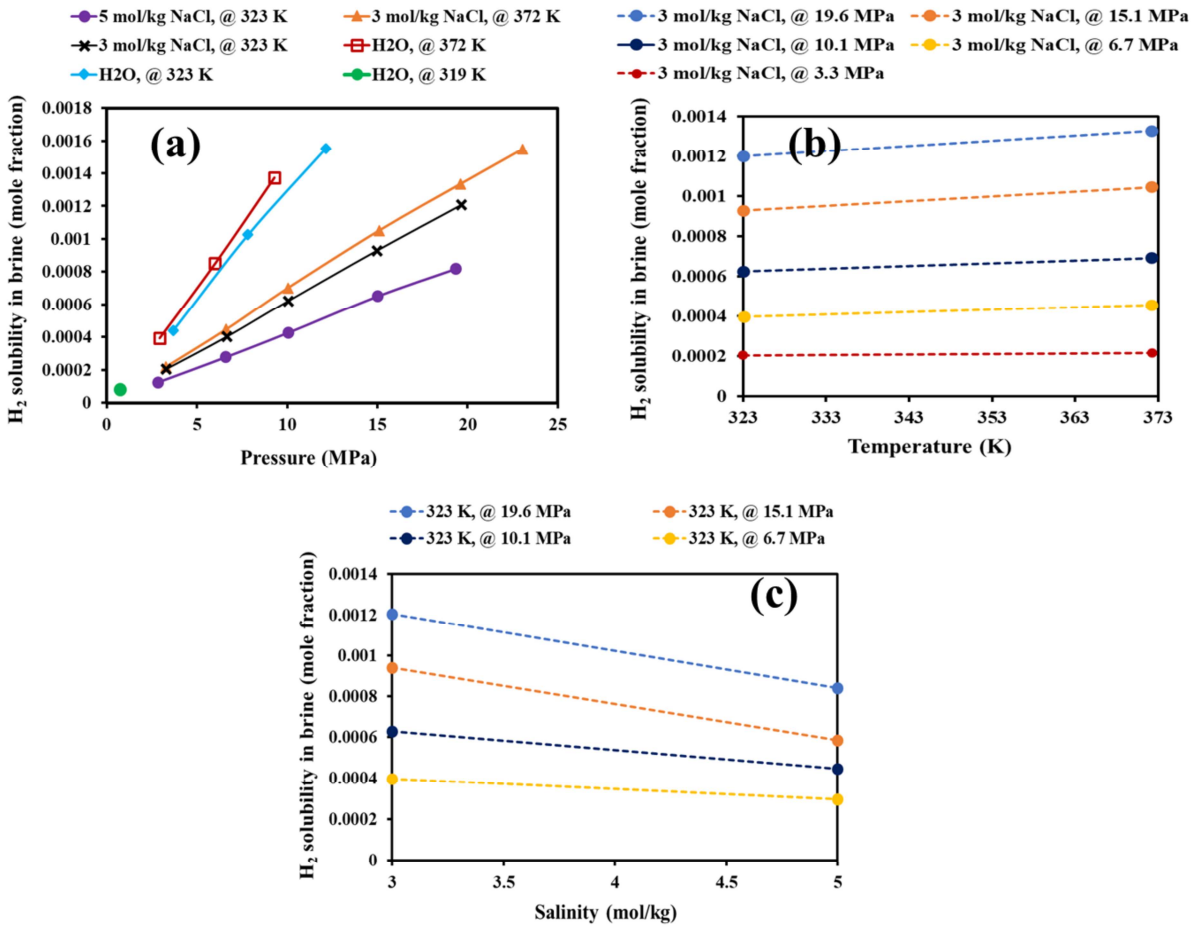

Fig. 2. H_2 solubility at different experimental conditions. Adapted from [52].

As anticipated, the solubility of hydrogen in water decreases in the presence of salt due to the salting-out effect [39,51]. This effect occurs because the salt ions compete with the gas molecules for space in the liquid, thereby decreasing the concentration of dissolved gas. However, the magnitude of the effect depends on the nature of the gas as well as the salt concentration. For example, the effect may be stronger for non-polar gases (as they do not have a permanent dipole moment) like H_2, CH_4, N_2, and CO_2 [53] than for polar gases (as they have a permanent dipole moment due to an uneven distribution of charge within the molecule, resulting in a partial positive and partial negative end) like CO, water [54]. Additionally, different salts may have different effects on gas solubility due to differences in ion size and charge. The H_2 solubility behavior with respect to brine concentration is often validated by models. Chabab et al. [41] and Torín-Ollarves and Trusler, [47] models for H_2 solubilities in pure water and at NaCl molalities below 0.5 mol NaCl/kg H_2O, as observed by van Rooijen et

al. [39]. However, for NaCl concentrations higher than 0.5 mol NaCl/kg H_2O, the two models are likely to predict different H_2 solubilities.

With respect to temperature, the solubility of hydrogen decreases as the temperature increases, possibly due to the shift in hydrogen's phase behavior. According to Rooijen et al. [39], despite the use of different force fields for Na^+, Cl^-, and H_2 gas, the models by Torín-Ollarves and Trusler, [47] and Lopez-Lazaro et al. [50] showed good agreement in terms of temperature. Furthermore, Gholami [51] in **Figure 3** compared the effect of monovalent ions (Na^+ and K^+) with that of divalent ions (Ca^{2+} and Mg^{2+}) in terms of temperature. The study showed that divalent ions have a greater impact on reducing the solubility of hydrogen in water compared to monovalent ions. Among the monovalent ions, K^+ was found to decrease the solubility more than Na^+, while among the divalent ions, Ca^{2+} had a stronger effect on the solubility than Mg^{2+}. This observation may be attributed to the size of the ions and their ionic energy in the solution [51]. This trend can be seen to decrease as the temperature increased from 50 ℃ to 100 ℃.

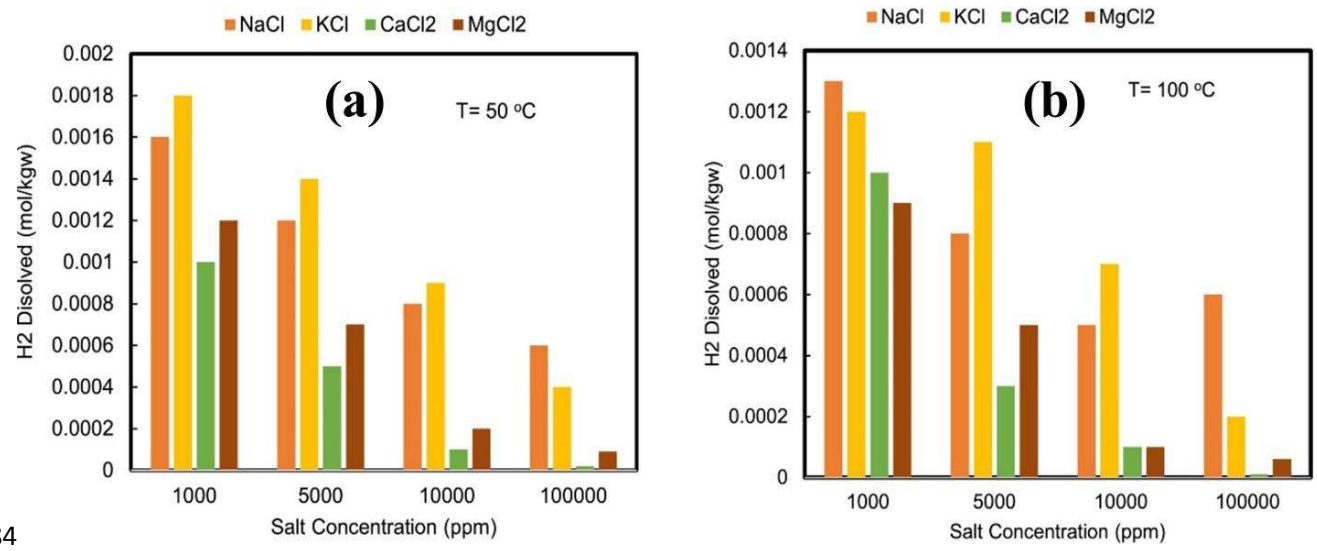

Fig. 3. Hydrogen solubility in brine for different salt types at 20 MPa for (a) 50 °C and (b) 100 °C [51].

Lastly, the effect of hydrogen solubility with increasing pressure is that it generally leads to an increase in the solubility of gases in liquids. This is because increasing pressure causes more gas molecules to be forced into the liquid, thereby increasing the concentration of dissolved gas in the liquid. However, the changes in solubility are influenced by the phase and thermodynamic behavior of hydrogen in relation to the ionic solution [51,55]. As a result, the relationship between solubility and pressure depends on the nature of the gas and the liquid.

3. Interfacial tension (IFT)

A phase boundary exists at the interface of H_2 and other fluids in the reservoir. A crucial characteristic of the phase boundary is the IFT amongst the several phases present in the reservoir. The IFT of H_2 in the presence of reservoir fluids determines the fluid behavior in the reservoir. Hence, this parameter is considered important for estimating the gas storage efficiency and crucial for the proper design of injection and withdrawal schemes [37]. To determine the IFT at the fluid-fluid interface, the pendant drop method is more commonly used. The procedure involves profile drop analysis of a fluid droplet (liquid) suspended from a needle in a chamber containing another fluid (gas).

3.1 Fluid-Fluid Interfacial Tension

Several factors impact the IFT of H_2 at the fluid-fluid interface. These include pressure, temperature, salinity, presence of organic acids, and cushion gas.

3.1.1 Effect of pressure

Pressure influences the intermolecular interaction between H_2 and other fluids in the reservoir. Increasing the pressure of the system causes the density of the gas to become higher and a corresponding decrease in IFT is obtained at the fluid-fluid interface. However, the pressure effect is considered infinitesimal on the IFT between H_2 and reservoir fluids [39]. This is often attributed to the low solubility of H_2 in brine. Moreover, H_2 has extremely low density. Higgs et al. [56] noted that increasing the pressure of the H_2-brine interface from 6.89 MPa to 20.68 MPa resulted in a minimal reduction of IFT at the interface from 72 mN/m to 69 mN/m. Chow et al. [57] conducted a comprehensive investigation of the IFT of (H_2 + H_2O) at varying temperatures and pressures. At a constant temperature (25 ℃), increasing the pressure of the system from 0.5 MPa to 45.2 MPa cause a slight reduction of the IFT from 72.3 mN/m to 68.7 mN/m (Figure 5). Also, Al-Mukainah et al. [58] observed a slight reduction in the H_2–brine interfacial tension ($\gamma_{\mathrm{H2-brine}}$) with an increase in the pressure of the system. At 14.7 psi, 63.68 mN/m was recorded for the ($\gamma_{\mathrm{H2-brine}}$) which decreased to 51.29 mN/m at 1,000 psi. Their

observation corroborated the study of Hosseini et al. [59] with increasing pressure on H_2-brine interfacial study as shown in **Figure 4**. Likewise, Esfandyari et al. [60] measured the IFT of H_2-distilled water at varying temperatures and pressures. At 80 ℃, the IFT of the H_2–H_2O interface decreased from 71.0 mN/m to 68.4 mN/m when the pressure of the system was raised from 10 to 100 bar, respectively. However, van Rooijen et al. [39] used molecular simulation to compute IFT between H_2/H_2O/NaCl as a function of pressure (1 – 600 bar), temperature (298 – 523 K) and salinity (0.6 M NaCl). In terms of pressure, their simulation result found no significant pressure dependence with IFT. More experimental and modeling studies are required to understand the impact of the pressure of IFT during UHS.

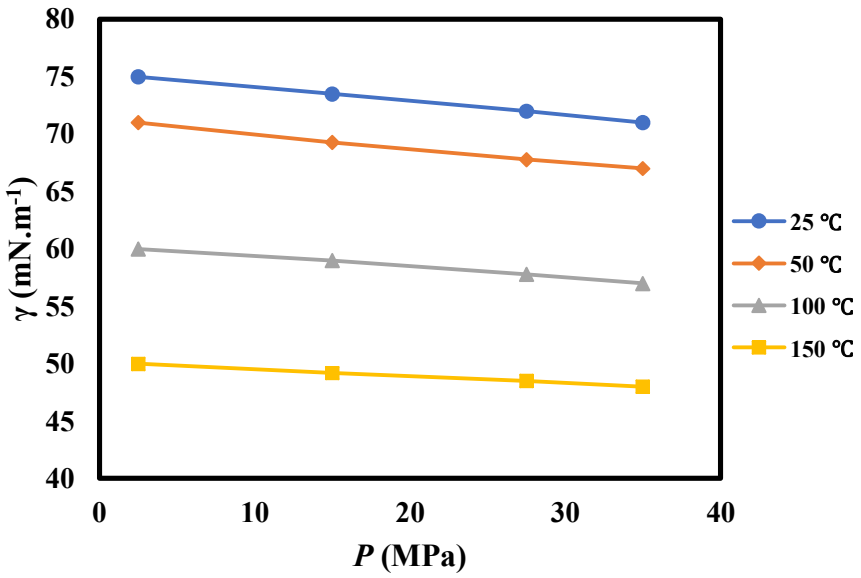

Fig. 4. Effect of pressure on the IFT of H_2-brine (brine molality = 1.05 mol./kg) [59].

3.1.2 Effect of temperature

As compared to pressure, increasing temperature causes the IFT of H_2-brine to decrease significantly [39]. The reduction in IFT with temperature is due to the higher thermal activities of the molecules of H_2 and the reservoir fluids which result in adhesive interaction between the fluids at the interface. Hosseini et al. [59] investigated the IFT of the H_2-H_2O interface at varying temperatures, pressures, and salinity conditions. At a constant pressure of 34.47 MPa, the IFT of the H_2-H_2O interface was lowered from 69.25 mN/m at 25 ℃ to 46.97 mN/m at 150 ℃. Similarly, at 10.1 MPa, Chow et al. [57] recorded the IFT of H_2-H_2O interface as 71.9 mN/m at 25 ℃, and 59.3 mN/m at 100 ℃, respectively. The recent work by van Rooijen et al. [39] observed a nonlinear decrease of IFT with increasing temperature. Their findings

corroborated the experimental data of Chow et al. [57] compared to Hosseini et al. [59] who reported a linear decrease of IFT with temperature. The authors reinforce their argument by highlighting that the IFT between two phases in contact is nonlinearly dependent on the density difference as noted by Poling et al. [61]. Additionally, since temperature also has a nonlinear effect on the density difference between H_2 and H_2O, it is logical to assume that the relationship between IFT and temperature will also exhibit nonlinear behaviour. Therefore, the nonlinear relationship between IFT and temperature observed by their simulation is not surprising [39]. In the case of H_2-brine IFT, Esfandyari et al. [60] observed a decrease in the IFT of H_2-brine interface with temperature. At constant pressure of 100 bar, the surface tension at the interface of H_2-brine decreased from 62.8 mN/m at 20 ℃ to 57.2 mN/m at 80 ℃, respectively. Similarly, Isfehani et al. [62] noted a reduction of the IFT of the H_2-CO_2-brine interface with an increase in temperature as shown in **Figure 5**. At constant pressure of 4,000 psi, the IFT of H_2-CO_2-brine reduced from approximately 70 mN/m at 23 ℃ to 56 mN/m at 100 ℃. Mirchi et al. [17] recorded the IFT of H_2-CO_2-brine at 1,000 psi as 70.36 mN/m, 68.04 mN/m, and 65.94 mN/m for 22, 40, and 60 ℃, respectively.

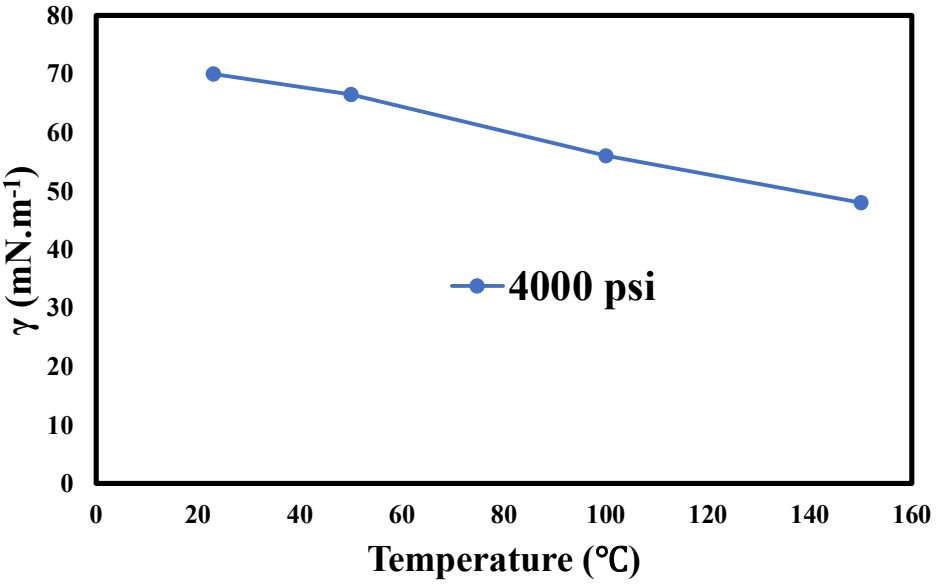

Fig. 5. Effect of temperature on the interfacial tension of H_2-brine interface at brine molality of 1.05 mol/kg. Adapted from [62].

3.1.3 Effect of salinity

Salinity has a pronounced effect on the IFT of the H_2-brine interface. Increasing salinity has been shown to cause the interfacial tension of the H_2-brine interface to increase. This is because

hydrogen solubility in brine decreases with increasing brine salinity [41]. Since there is more salt packed into the water, salinity notably increases the density of the brine. Meanwhile, H_2 is characterized with a lower density. Thus, the induced high differential density ($\Delta\rho$) causes a higher IFT [59]. At constant temperature and pressure (323 °K, 20 MPa), the solubility of H_2 in 1,000 ppm and 5,000 ppm NaCl brine is 0.0016 and 0.0012 mol/kg, respectively (refer to **Figure 3(a)**) [51]. Divalent ion concentration further reduces the solubility of H_2 gas in brine. Hosseini et al. [59] studied the effect of salinity on the IFT of the H_2-brine interface. As illustrated in **Figure 6**, the interfacial tension of the H_2-brine interface becomes higher with increasing molality of the brine. van Rooijen et al. [39] via molecular investigation also observed a linear increase of IFT with solution molalities. Besides density difference (since the density of saline H_2O is greater than pure H_2O), they observed that ions arrangement (cations and anions) at the interface can play a significant role in promoting a linear increase of IFT with salinity [63–68]. Specifically, cations strengthen the hydrogen bond network of H_2O while anions have the opposite effect, leading to cations being absorbed into the bulk phase and anions being depleted from it [63,66,67]. Overall, the network of hydrogen bonds becomes toughened and rigid, thereby increasing the IFT [64,65].

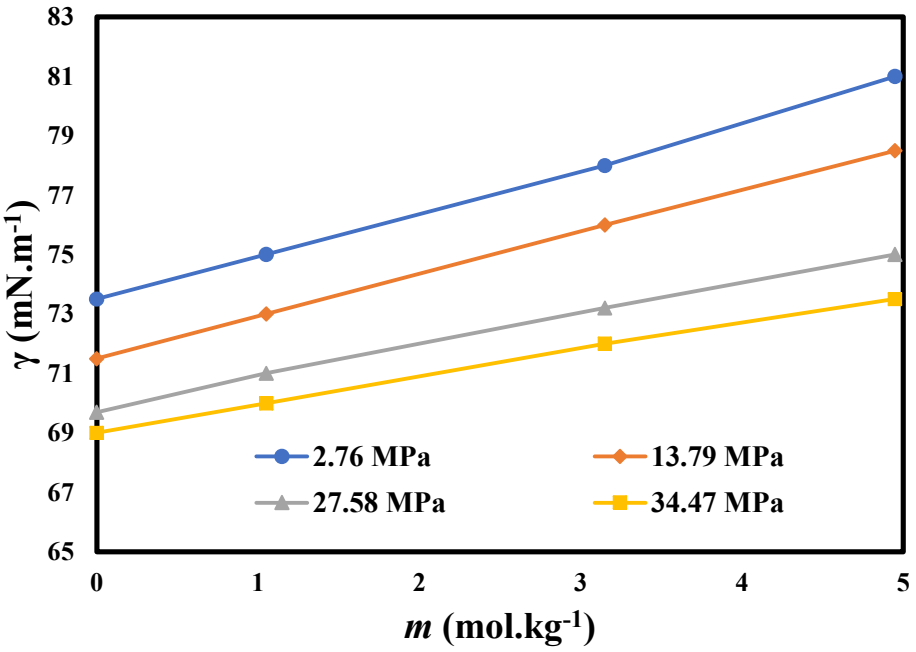

Fig. 6. Effect of salinity on IFT of H_2-brine interface. Adapted from [59].

3.1.4 Effect of cushion gas

283 To improve the injection scheme and withdrawal efficiency of hydrogen in underground
284 geologic porous media, cushion gas has been proffered as supplementary gas to be injected
285 ahead of the working gas (in this case H_2 gas). CH_4, CO_2, and N_2 have been evaluated as
286 cushion gas during UHS. The injected cushion gas acts as a buffer to provide pressure during
287 the storage process, thereby enhancing H_2 gas deliverability during the withdrawal cycle [69].
288 Zamehrian and Sedaee [70] performed numerical simulations to study the role of cushion gas
289 during the hydrogen storage process in a gas condensate reservoir. They noted that the use of
290 N_2 gas improved reservoir pressure, and consequently H_2 gas recovery efficiency. Nonetheless,
291 the introduction of cushion gas with H_2 into geological formations influenced the reservoir
292 hydrodynamics due to unavoidable gas mixing and molecular diffusion. Hence, it is crucial to
293 understand the effect of the cushion gas on the fluid-fluid interactions with H_2 gas.

294 Mirchi et al. [17] conducted IFT studies of H_2 – CH_4/brine mixtures at typical reservoir
295 conditions. The composition of cushion gas in the mixture was varied from 20% to 100% CH_4.
296 Increasing cushion gas concentration caused a reduction in the IFT at the H_2-brine interface.
297 At constant temperature and pressure (60 ℃ and 1,000 psi), the IFT of 80% H_2 - 20% CH_4 is
298 65.24 mN/m while the IFT of 50% H_2 - 50% CH_4 is 62.46 mN/m. Further increasing the CH_4
299 concentration to 80% caused the lowering of IFT to 56.41%. The lower IFT recorded for the
300 H_2 – CH_4 mixture was ascribed to the better solubility of CH_4 in brine, which caused greater
301 interaction between them at the interface. Similarly, Isfehani et al. [62] examined the IFT of
302 H_2-CO_2-brine mixtures. The IFT of H_2-CO_2-brine mixtures decreases with increasing
303 concentration of CO_2 as illustrated in **Figure 7**. At 50 ℃, brine molality of 1.05 mol/kg, and
304 2,000 psi pressure, the IFT of 70% H_2- 30% CO_2 mixture is 55.64 mN/m while the IFT of 30%
305 H_2- 70% CO_2 mixture is 34.87 mN/m. This was attributed to the increase in the density of the
306 gas mixture and consequently, a reduction in the density difference between the water solution
307 and gas mixture.

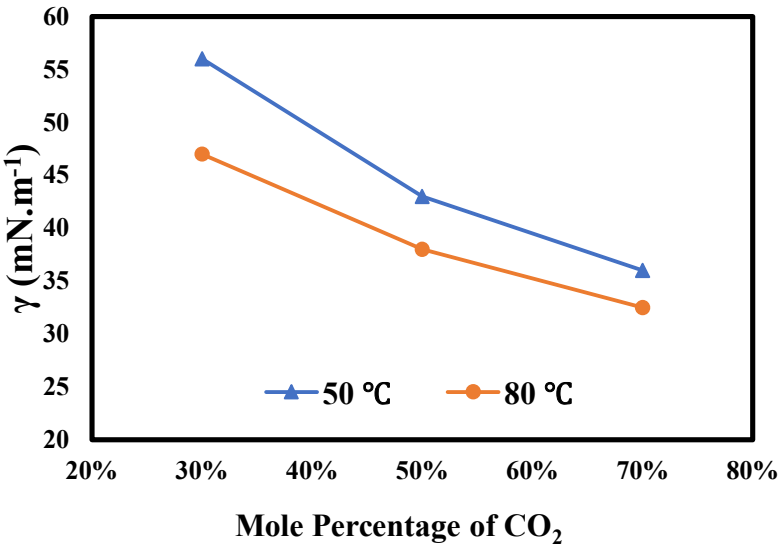

Fig. 7. IFT of H_2-CO_2 mixtures, molality = 1.05 mol/kg. Adapted from [62].

Alanazi et al. [72] recently conducted a study to investigate the IFT of H_2-CH_4/brine mixtures with the addition of 2 wt.% NaCl and 1 wt.% KCl. The study was carried out at a temperature of 323 K and pressures ranging from 0.1 to 1600 psi to assess the possibility of using CH_4 as a cushion gas for structural and residual trapping. As shown in **Figure 8(a)**, the change in CH_4/brine IFT with increasing pressure was more pronounced than that of H_2/brine IFT. The study found that the CH_4/brine IFT decreased rapidly after 400 psi due to the attainment of critical CH_4 conditions (i.e., 673 psi and 190.55 K). The study also revealed that the highest IFT values were recorded in pure H_2, while the pure CH_4/brine IFT values were the lowest. For instance, at a temperature of 323 K, the IFT value of pure H_2/brine showed a minor decline from 55 to 53 mN/m, whereas the CH_4/brine IFT values reduced from 54.5 to 46.5 mN/m with an increase in pressure from 200 to 1600 psi. The IFT values of H_2-CH_4/brine were found to be intermediate between those of pure H_2 and pure CH_4. The difference in density between pure CH_4, CH_4-H_2 mixture, and pure H_2 (illustrated in **Figure 8(b)**) may account for the lower IFT values recorded in pure CH_4/brine and H_2-CH_4/brine compared to pure H_2/brine. This can be attributed to improved intermolecular interactions in pure CH_4 and CH_4-H_2 molecules at the interface compared to the H_2/brine system. The authors suggest that the use of a cushion gas (such as CH_4) before H_2 injection into geological storage formations could result in reduced capillary pressure by decreasing IFT and increasing contact angles (as discussed in **section 4**). However, this raises the possibility of H_2 diffusing across the caprock at the mixing zone between the cushion gas (H_2-CH_4 mixture) and stored gas. **Table 1** summarizes the discussed fluid-fluid IFTs, including the H_2-water, H_2-brine, H_2-CH_4 brine, and H_2-CO_2 brine systems.

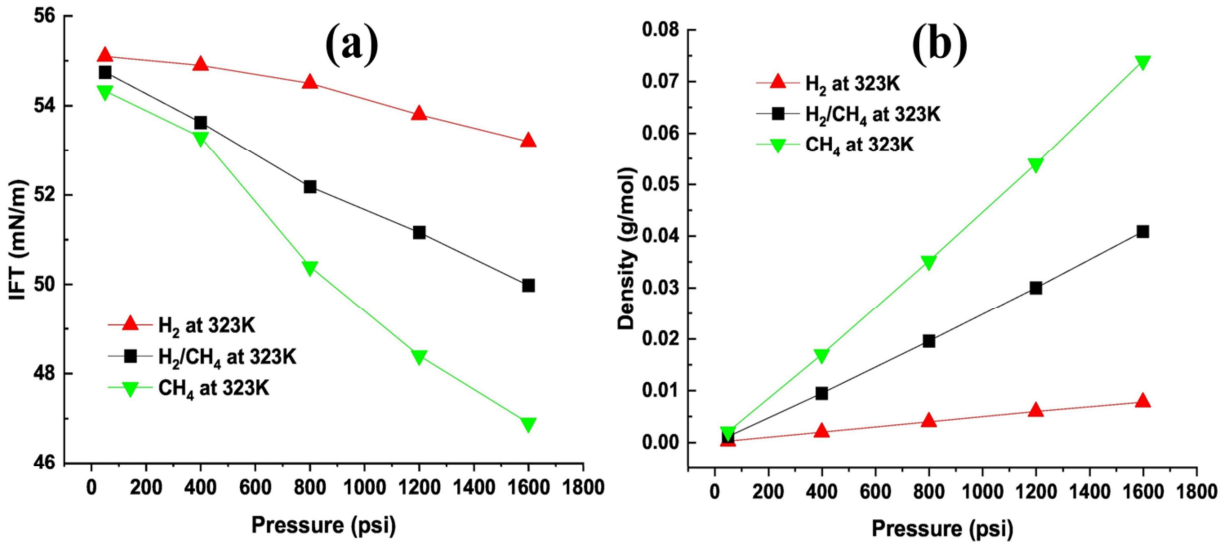

331

332 **Fig. 8**. (a) Measured IFT values between gas and liquid (10 wt% NaCl brine) for H_2/brine, CH_4/brine,
333 and H_2-CH_4/brine mixture (50 %/50 %) systems at different pressures (50–1600 psi) and 323 K with an
334 uncertainty range of ±1.7 to ±2.3 mN/m. (b) Density values of H_2/brine, CH_4/brine, and H_2-CH_4/brine
335 mixture (50 %/50%) systems at varying pressures (50–1600 psi) and 323 K [71].

336 **Table 1.** Summary of existing literature on Fluid-Fluid IFT.

Reference	Methods	Gas type (s)	Pressure (MPa)	Temperature (K)	Salinity (wt.%)	Concluding Remarks
Chow et al. [57]	Pendant	$H_2 + H_2O$, $H_2 + CO_2 + H_2O$	0.5 – 45	298.15 – 448.15	Pure water	• The interfacial tension exhibited an initial rise followed by a subsequent decline as pressure increased.
Higgs et al. [56]	Pendant	H_2	0.68 – 1.71 & 6.88 – 20.67	298.15	Pure water, 0.1/0.2/ & 0.5 NaCl brine	• At high pressure, the interfacial tension showed a reduction in response to changes, while salinity had no discernible impact on the interfacial tension. • No notable correlation between the interfacial tension and salinity for solutions containing 0.1 wt.% and 0.5 wt.% NaCl.
Hosseini et al. [59]	Pendant	H_2	2.75, 13.78, 27.57, 34.47	298.15, 323.15, 373.15, 423.15	Deionized water, (0.864 moles NaCl + 0.136-moles KCl)	• The interfacial tension demonstrated a linear decrease with both pressure and temperature while exhibiting an increase in salinity.

Esfandyari et al. [60]	Captive	H_2	1 – 10	293.15 – 353.15	Distilled water and formation brine (NaCl, KCl, $CaCl_2$, and $MgCl_2$)	• For the H_2-water system, the interfacial tension displayed an increase with temperature and salinity, but a decrease with pressure. • The interfacial tension decreased with both temperature and pressure for the H_2-formation brine systems.
Al-Mukainah et al. [73]	Pendant	H_2	0.1 – 6.89	323.15	Brine, 10 NaCl	• The interfacial tension exhibited a minor reduction in response to changes with increasing pressure.
Mirchi et al. [17]	Pendant	H_2, CH_4, H_2–CH_4 mixture	6.89	295.15, 313.15, 333.15	Brine, 2 NaCl	• As the temperature increased, the interfacial tension between H_2-CH_4 and brine decreased. • The interfacial tension between H_2-CH_4 and brine decreased as the fraction of H_2 decreased (i.e., an increase with CH_4 fraction).

Dalal Isfehani et al. [62]	Pendent	H_2-CO_2 mixture	3.45, 8.27, 13.78 and 20.68	323.15 and 353.15	0.864 NaCl + 0.136 KCl	• The interfacial tension decreased in a linear trend as pressure and temperature increased while showing an increase with salinity. • As the fraction of CO_2 increased, the interfacial tension between H_2-CO_2 and brine decreased.
Alanazi et al. [71]	Pendant	H_2, CH_4, H_2–CH_4 mixture	0.00068 to 11.03	323.15	Brine, 2 NaCl Brine, 1 KCl	• The interfacial tension decreased in the following order: H_2/brine > H_2-CH_4/brine > CH_4/brine.
van Rooijen et al. [39]	Molecular simulation	H_2	0.1 – 60	298 – 523	0 – 6 NaCl molalities/kg	• There was no discernible correlation between pressure and the interfacial tension. • An inverse relationship was observed between the interfacial tension and temperature, with a non-linear decrease as temperature increased. • The interfacial tension demonstrates a linear increase in

						response to changes in solution molalities. • The results exhibited excellent agreement with experimental data, with a deviation of only 10% observed for the majority of data points. • Findings could serve as data sets for the development of engineering equations that captures the effect of pressure, temperature, and solution molality for wide UHS applications.

337

It is noteworthy that despite the advantages of using cushion gas during UHS, the excessive introduction of cushion gas is highly discouraged. This is because it has the potential of reducing hydrogen purity [74]. Moreover, a high concentration of cushion gas has the potential of limiting the structural trapping, and may negatively impact the integrity of injection and withdrawal wells [17,75]. Hence, more studies are needed to determine the optimum concentration of cushion gas that is required to safely store H_2 in geological formations and offer the required pressure for high H_2 recovery efficiency. Additionally, previous studies have highlighted the role of N_2, CO_2, and CH_4 as cushion gas for UHS with varying degrees of efficiency [17,70]. The limitation of utilizing these gases has been identified as unavoidable mixing which may ultimately result in hydrogen loss. Currently, there is no study that quantifies the amount of hydrogen loss encountered from the unavoidable mixing of H_2 gas with the existing cushion gases. Moreover, more gases with a lower tendency for unavoidable mixing during their H_2 storage and withdrawal are desired and recommended for future research.

Overall, studies on fluid-fluid interaction between H_2 and reservoir fluids are very few in the literature. More studies of the interaction between hydrogen and formation brine are required to ascertain their interaction at the pore scale. More importantly, previous studies have only established the effect of individual salts as representative of reservoir brine. However, the formation brine in reservoirs is usually a mixture of monovalent, divalent, and sometimes trivalent cations. Future studies should consider the effect of the formation's brine-containing salt mixture on H_2-brine IFT behavior. Furthermore, hydrocarbon reservoirs (especially depleted reservoirs) contain organic acids. The solubility of H_2 in organic acid differs from aqueous solutions. Hence, the effect of organic acid concentration on the IFT of H_2-brine should be considered for further studies.

3.2 Rock-fluid interfacial tension

The importance of rock-fluid IFT during UHS cannot be overemphasized as it determines the fluid-spreading behavior of H_2 gas on reservoir-rock systems [32]. Besides, rock-fluid IFT dictates the distribution and migration of H_2 gas in the underground reservoir [52]. Unlike fluid-fluid IFT which is easily determined experimentally, there is currently a lack of experimental methods to effectively estimate rock-fluid IFT. Hence, semi-empirical methods and

correlations such as Young's equation and Neumann's equation of state are used to determine the rock-fluid IFT.

3.2.1 Effect of temperature and pressure

Temperature and pressure are critical parameters that affect the rock-fluid IFT. Several studies posited that the IFT of rock-H_2 decreases with increasing temperature and pressure. Increasing pressure causes the density of gas to increase and resultantly the rock-H_2 intermolecular forces. Consequently, the IFT of the gas at the rock surface is lowered. In similitude to the effect of pressure, higher temperature causes the kinetic energy of H_2 gas to increase. Resultantly, the mobility of H_2 gas increases, thereby having less time to react with the solid surface [32]. Pan et al. [76] evaluated the rock-fluid IFT of H_2 gas interaction with clean quartz rock using a semi-empirical method. They noted that the IFT of the rock-fluid ($\gamma_{\mathrm{rock-fluid}}$) interface decreases with an increase in the temperature and pressure of the geologic medium. At 50 ℃, the $\gamma_{\mathrm{quartz-}\ _2}$ decreased from 101 mN/m to 88 mN/m when the pressure is raised from 5 MPa to 25 MPa. Similarly, at constant pressure of 20 MPa, increasing the temperature from 50 ℃ to 70 ℃ caused the $\gamma_{\mathrm{quartz}-H_2}$ to decrease from 92 mN/m to 83 mN/m.

Additionally, Ali et al. [77] observed that at 50 ℃, the IFT of mica-H_2 reduces from 114 mN/m to 95 mN/m when the pressure is increased from 5 MPa to 20 MPa as illustrated in **Figure 9**. Also, at a constant pressure of 10 MPa, the IFT of mica-H_2 reduced from 111 mN/m to 102 mN/m when the temperature condition was increased from 35 to 70 ℃. Yekeen et al. [78] applied Neumann's equation to understand the impact of temperature and pressure on clay-hydrogen interfacial tension. At 60 ℃ and 5 MPa, the IFT for $\gamma_{\mathrm{montmorillonite}-H_2}$ is recorded as 67 mN/m; whereas the IFT decreased to 58 mN/m at 20 MPa. Also, the IFT of $\gamma_{\mathrm{quartz}-H_2}$ decreased from 100 mN/m at 5 MPa to 94 mN/m at 20 MPa. Furthermore, Esfandyari et al. [79] quantified the $\gamma_{\mathrm{rock}-H_2}$ as a function of temperature and pressure. At 40 ℃, the $\gamma_{\mathrm{basalt}-H_2}$ decreased from 72.01 mN/m to 68.00 mN/m while the $\gamma_{\mathrm{gypsum}-H_2}$ reduced from 64.07 mN/m to 59.66 mN/m when the pressure of the system was adjusted incrementally from 10 to 100 bars.

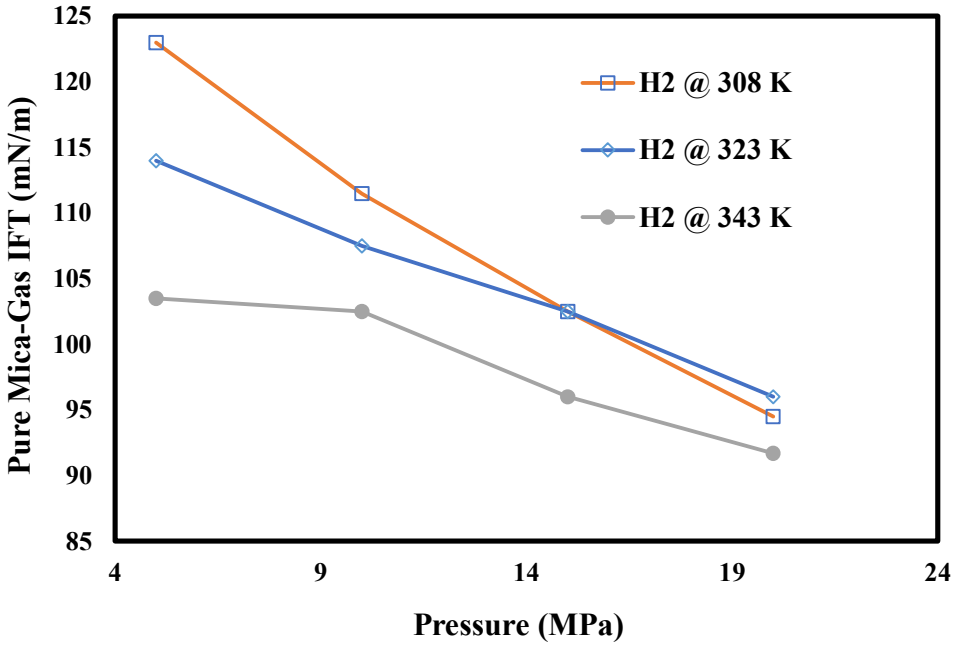

396

397 **Fig. 9.** Effect of temperature and pressure on the IFT of mica-H_2 interface. Adapted from
398 [77].

399 ***3.2.2 Effect of stearic acid concentration***

400 An increase in the concentration of organic acid causes the $\gamma_{\text{rock-H2}}$ to decrease. This is
401 because the presence of organic acid increases the hydrophobicity of the system which prevents
402 water from attaching to the surface. Nonetheless, H_2 can easily attach to the surface as it
403 contains no external dipole moment. Hence, less energy is required by H_2 gas to interact with
404 the surface. Pan et al. [76] investigated the role of organic acid on the rock-fluid IFT of quartz
405 and H_2 gas and compared the effect to CO_2. As illustrated in **Figure 10**, at constant temperature
406 and pressure (50 ℃ and 25 MPa), increasing the concentration of stearic acid from 10^{-9} to
407 10^{-2} mol/L decreased the $\gamma_{\text{quartz}-H_2}$ from 85 mN/m to 72 mN/m. Likewise, Hosseini et al.
408 [80] determined the $\gamma_{\text{rock-fluid}}$ of calcite-H_2 interface at constant temperature and pressure (50
409 ℃, and 10 MPa). They observed that the $\gamma_{\text{calcite-H2}}$ decreased significantly from 71.77 mN/m
410 to 29.26 mN/m when the organic acid concentration is raised from 10^{-9} to 10^{-2} mol/L.

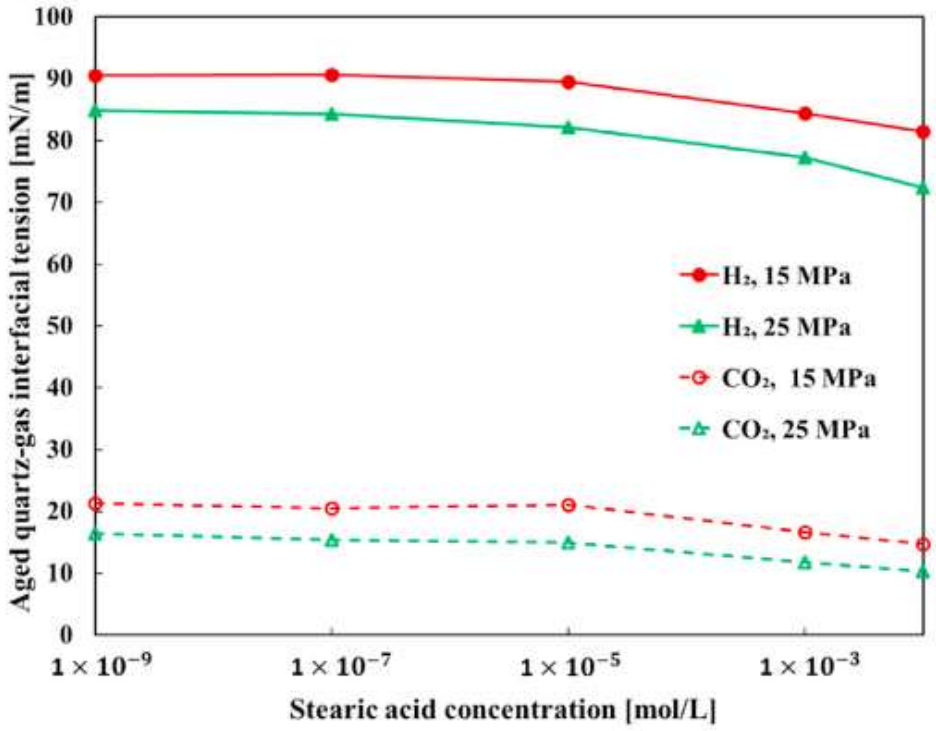

411

412 **Fig. 10.** Effect of stearic acid on the IFT of quartz-H_2. Adapted from [76].

413 ***3.2.3 Effect of salinity***

414 An increase in the ionic strength increases the $\gamma_{rock-fluid}$ especially at lower temperatures.
415 Hosseini et al. [80] measured the effect of salinity on $\gamma_{rock-flui}$ using empirical methods. At
416 constant temperature and pressure, an increase of the salinity from 0 to 4.95 mol/kg cause the
417 $\gamma_{rock-fluid}$ of H_2-water system to increase from 50 mN/m to 57.17 mN/m. Similarly,
418 Esfandyari et al. [79] studied the rock-fluid IFT of mineral/H_2/H_2O via theoretical methods. At
419 40 ℃ and 10 MPa, the $\gamma_{calcite-H2}$ in distilled water was recorded as 33.02 mN/m while the
420 $\gamma_{calcite-H2}$ in brine was recorded as 47.89 mN/m. Comparably, at the same temperature and
421 pressure, the $\gamma_{quartz-H2}$ was 16.52 mN/m and 28.79 mN/m in distilled water and brine,
422 respectively. This was attributed to the adsorption of the dissolved ions of the brine to the rock
423 surface, thereby causing an increase in the surface charge and a reduction in the polarity at the
424 rock surface. Consequently, the van der Waal's forces on the rock surface decrease whereas
425 the IFT of the rock-H_2 gas increases.

426

427

3.2.4 Effect of rock mineralogy

Rock mineralogy has a significant effect on rock-fluid IFT. Pan et al. [76] assessed the rock-fluid IFT of H_2 gas interaction with clean quartz and basaltic rock using a semi-empirical method. At the same temperature and pressure (50 °C and 10 MPa), the $\gamma_{\text{rock}-H_2}$ for clean quartz is 100 mN/m while the $\gamma_{\text{rock}-H_2}$ for basaltic rock is 75 mN/m. The observed difference recorded in the IFT for the two rocks was ascribed to the presence of organic matter in the basaltic rock. This is consistent with the previous discussion of the role of organic acid on the rock-fluid IFT. Similarly, Yekeen et al. [78] investigated the impact of rock mineralogy on rock-fluid IFT for quartz and clay surfaces. At 5 MPa and 60 °C, the $\gamma_{\text{quartz}-H_2}$ was recorded as 100 mN/m while the $\gamma_{\text{montmorillonite}-H_2}$ is recorded as 67.26 mN/m. This was ascribed to the high quantity of silanol function group on the surface of quartz which implies minimal available sites for interaction with H_2. Besides, the $\gamma_{\text{kaolinite}-H_2}$ and $\gamma_{\text{illite}-H_2}$ was recorded as 68.64 mN/m and 67.89 mN/m, respectively (see **Figure 11**). The high IFT recorded during interaction of clay-H_2 is indicative of minimal interaction between the clay mineral and H_2 gas. Since caprock of most geological structure consists of clay and mudstone, the similar IFT of the rock-H_2 interface means the UHS is unlikely to be affected by change in clay composition.

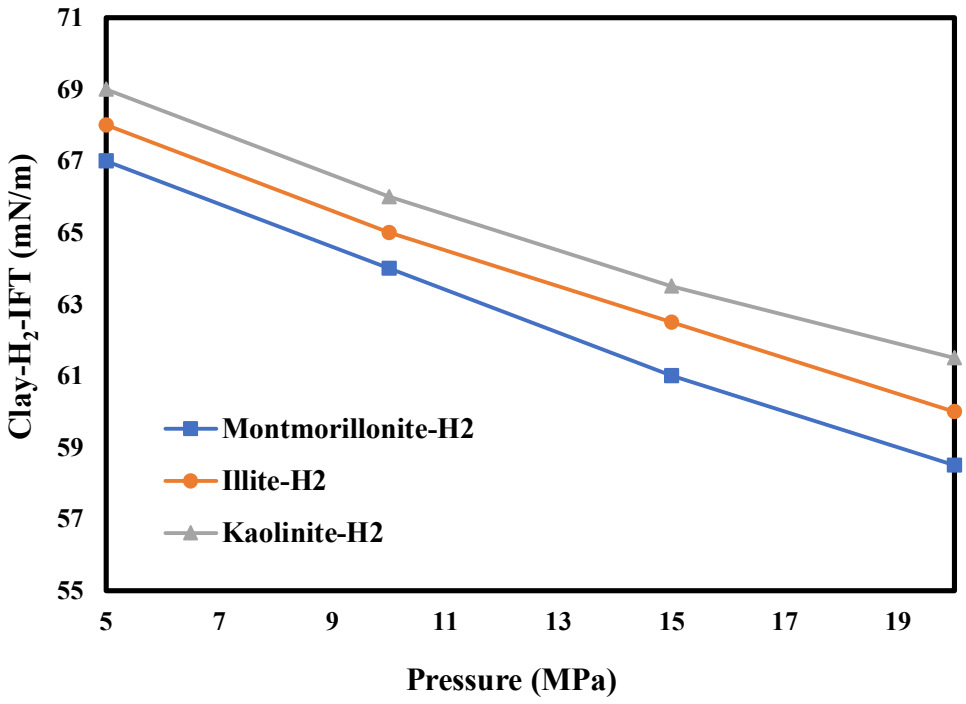

Fig. 11. Predicted H_2-clay interfacial tension as a function of pressure for montmorillonite, illite and kaolinite at 60 °C. Adapted from [78].

447 Overall, rock-fluid IFTs are quite tedious to compute, however, the use of these empirical
448 methods and correlations can help reduce the level of uncertainties in establishing relevant data
449 for UHS application. **Table 2** therefore, summarizes the discussed rock fluid (i.e., rock/H_2 and
450 rock/brine) IFT experiments.

451 **Table 2.** Summary of existing literature on rock fluid (i.e., rock/H_2 and rock/brine) IFT experiments.

Reference	Methods	Substrates type (s)	Gas type (s)	Pressure (MPa)	Temperature (°C)	Salinity (wt.%)	Concluding Remarks
Pan et al. [76]	Semi-empirical method (Young's & Neumann's equation of state)	Quartz and basalt	H_2. CO_2, and CH_4	5 – 25	27, 50, 70	Nil	• The interfacial tension between rock and gas decreases as pressure and organic acid concentration increase. • At comparable thermophysical conditions, the order of priority for rock-gas interfacial tension is as follows: rock/H_2 > rock/CH_4 > rock/CO2.
Ali et al. [77]	Experiment (tilted plate method) and semi-empirical (Young's & Neumann's equation of state)	Mica	H_2	5 – 20	35 – 70	Brine, 10 NaCl	• The interfacial tension between solid and gas decreases with pressure, as well as with the increase in alkyl chain length and organic acid concentrations.
Hosseini et al. [81]	Experiment (pendant drop) and semi-empirical (Young's	Shale, evaporite,	H_2	5 – 20	25 – 80	0.864 mol NaCl + 0.136 mol KCl	• The interfacial tension between rock and gas decreases with increasing pressure,

	& Neumann's equation of state)	and basaltic rocks					temperature, and total organic carbon (TOC) content in shale. • At higher temperatures, rock-water interfacial tension decreases, whereas it increases with an increase in shale total organic carbon (TOC).
Yekeen et al. [78]	Semi-empirical	Kaolinite, llite and montmorillonite	H_2, N_2, and CO_2	5 – 20	60	Brine, 20 NaCl and 1 KCl	• Rock–gas interfacial tension for the investigated gases decreased in the order: Clay/H_2 > Clay/N_2 > Clay/CO_2. • For the clay minerals, the interfacial tension decreased in the manner: kaolinite/gas > illite/gas > montmorillonite/gas.
Esfandyari et al. [79]	Experiment (pendant drop) and semi-empirical (Young's & Neumann's equation of state)	Calcite, Dolomite, Quartz, Basalt, Granite, Shale,	H2	1 - 10	20 to 80	Distilled water and Formation water (48.75%	• The interfacial tension between rock and water increased with temperature but remained unaffected by changes in pressure.

		Anhydrite, and Gypsum				NaCl, 31.49% KCl, 7.12% $CaCl_2$, and 12.64% $MgCl_2$)	• The interfacial tension between rock and water showed a decrease with increasing salinity for calcite, dolomite, and quartz. • The interfacial tension between rock and water increased with salinity in basalt, granite, and gypsum. • The effect of pressure on rock-gas interfacial tension was a decrease, but its relationship with temperature was unpredictable. • The interfacial tension of the rock-gas was found to increase with salinity in all mineral types studied.

452

4. Wettability

A key and crucial factor during UHS is the wettability property of the rock. This parameter dictates the fluid distribution in the reservoir rock system and determines the fluid-flow behavior, trapping potential, storage capacity, and caprock sealing capacity during UHS [59]. To measure the wettability of rocks and substrates, several methods have been used. These include the sessile drop method, titling plate method, Wilhelmy plate method, capillary-rise method, capillary penetration method, captive bubble method, and micro-computed tomography imaging method [37]. The wettability property of the H_2-rock system is governed by several parameters. These include temperature, pressure, salinity, surface roughness, the presence of organic acid, and surface contamination. Generally, for caprock which is responsible for structural trapping during UHS, a more water-wet and less H_2-wet environment is favored to de-risk the UHS storage process. Besides, the low density of H_2 gas and its low solubility in brine enable its transportation during injection and withdrawal schemes. **Table 3** presents the summary of the wettability studies of the H_2–brine–rock system.

4.1 Effect of Salinity

Depleted reservoirs being considered for UHS contains inherent formation brine salinity which may have a considerable impact on the storage process. Hence, it is pertinent to consider the impact of brine salinity on H_2-Brine-rock wettability. Higgs et al. [56] estimated the wettability of H_2/brine/quartz at varying NaCl concentrations (0.1, 0.2, and 0.5 wt.%). They observed a weak correlation to no correlation between contact angle and brine salinity at low pressures and high pressures, respectively. Likewise, Hashemi et al. [82] utilized the captive bubble technique to evaluate the wettability of a H_2/brine/sandstone rock system. The authors conducted the experiments close to *in situ* conditions and observed that varying the salinity of the system is insignificant on the wettability of the sandstone rock surface. Esfandyari et al. [60] conducted wettability experiments of H_2/brine/rock in distilled and formation water brine at constant temperatures and pressures. At ambient conditions, the change in the salinity gradient only yielded an infinitesimal increase in the contact angle (CA) of the H_2/brine/rock system.

On the other hand, Zeng et al. [83] conducted surface complexation modelling to investigate the role of salinity on the H_2-rock wettability behaviour of carbonates by calculating the calcite surface potential to predict the structural disjoining pressure. They noted that the disjoining

pressure decreases with increasing salinity which consequently causes the contact angle to increase, and the calcite system became H_2-wet. Similarly, Hosseini et al. [84] noted that the increase of brine salinity of H_2/brine/rock for a carbonate rock from 0 mol/kg to 4.95 mol/kg resulted in an increase in the CA of the system. At 50 ℃ and 15 MPa, the advancing CA increased from, 69.8° to 80.65° while the receding CA increased from 63.35° to 73.3°. The dewetting of the surface was ascribed to reduced surface polarity resulting from the increase in salinity.

Hou et al. [85] conducted a comprehensive investigation on the effect of salinity on H_2/brine/rock wettability of carbonate rock surfaces. As illustrated in **Figure 12**, an increase in the solution salinity caused the water contact angle to increase, and consequently a decrease in the water wettability. Moreover, at the same concentration, the type of ions also influences the H_2 wettability of the surface. For example, the presence of potassium (K^+) ions causes more de-wetting of the surface compared to sodium (Na^+) ions. This is adduced to the higher atomic size of K^+ ions which causes more compression of the electrostatic double layer compared to Na^+ ions. Furthermore, the presence of divalent ions increases the H_2/brine/rock wettability of the carbonate rock surface. At 5.0 wt.% concentration, the advancing contact angles of $\theta_a =$ 71.3°, and 109.5° were recorded for NaCl, and $CaCl_2$, respectively. This is attributed to the more electropositive nature of the divalent cations. Besides, higher adsorption of the divalent cations will occur on the carbonate rock surface compared to the monovalent ions.

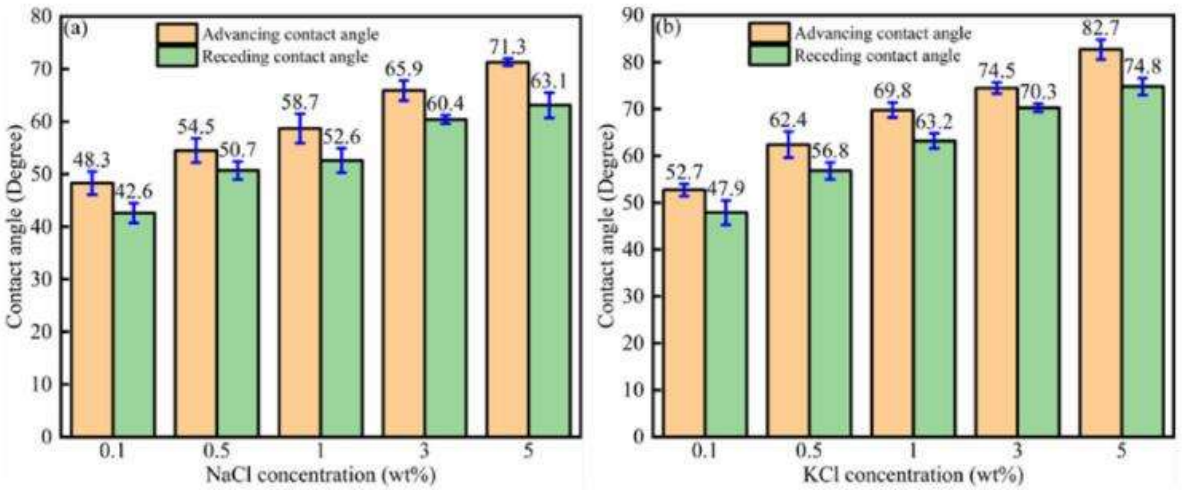

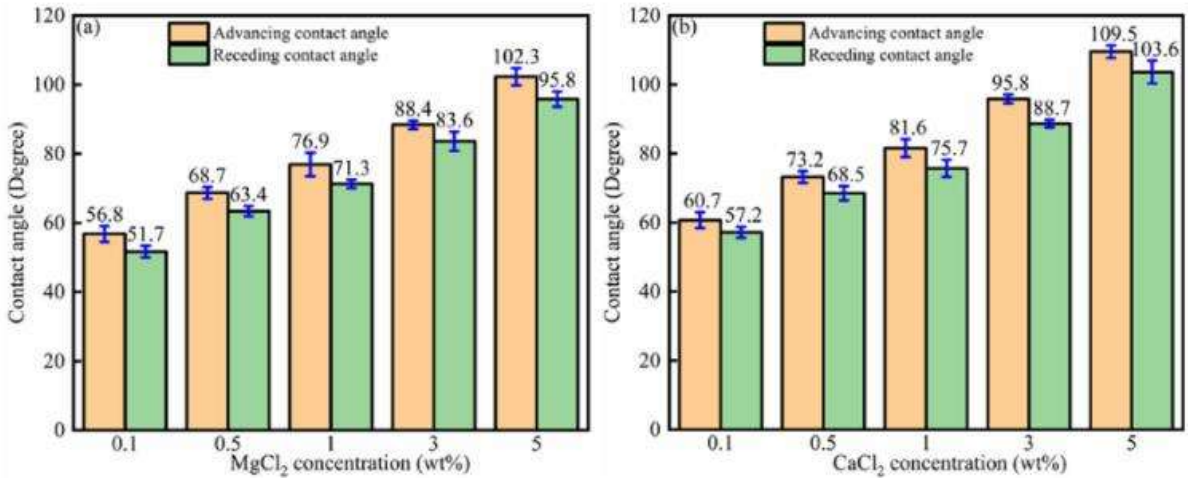

Fig. 12. Effect of monovalent and divalent ion concentration on the H_2/brine/carbonate rock wettability. Adapted from [85].

Overall, existing data reported in the literature for the effect of salinity on the wettability of H_2/brine/rock is inconsistent. While some authors reported that salinity has no effect on the wettability of the H_2/brine/rock system, other researchers noted infinitesimal to significant changes. Moreover, previous studies of the impact of salinity have mostly used individual salt concentrations (e.g., NaCl) to represent formation brine. This is at variance to real field conditions where the formation brine consists of a mixture of several salts. Indubitably, more studies of the impact of salinity on H_2-brine-rock wettability are required to de-risk UHS projects.

4.2 Effect of Pressure

An increase in the system pressure causes the density of H_2 gas to increase. Consequently, an increase in the intermolecular interaction H_2/brine/rock occurs, and this is accompanied by an increase in the contact angle [86]. Hosseini et al. [84] observed an increase in the CA of calcite rock with an increase in pressure. At 25 ℃, the advancing CA, $\theta_a = 0°$ at 0.1 MPa, indicative of strongly water-wetting condition. This changes to $\theta_a = 83.6°$ at 20 MPa corresponding to an intermediate wetting condition. Also, Iglauer et al. [87] noted an identical trend of increasing CA with an increase in the pressure on a quartz surface. Ali et al. [77] investigated the effect of pressure on the equilibrium CA of a H_2/brine/mica system. They remarked that the equilibrium CA increased at higher pressures. Likewise, Ali et al. [88] reported that raising the pressure from 15 MPa to 25 MPa causes the wettability of mica aged with hexanoic acid to increase from 67.5° to 80.3°. Similarly, an increase in the wettability of the mica substrate was

recorded for lauric acid and lignoceric acid whose advancing contact angle changed from 75.4° to 89.2°, and 91.8° to 106.2°, respectively. Al-Yaseri et al. [89] deduced the wettability of H_2/brine/shale using a semi-empirical thermodynamic model at typical geo-storage conditions. The authors acknowledged that increasing the pressure from 5 MPa to 20 MPa resulted in an increase in the hydrogen wettability of shale (see **Figure 13**).

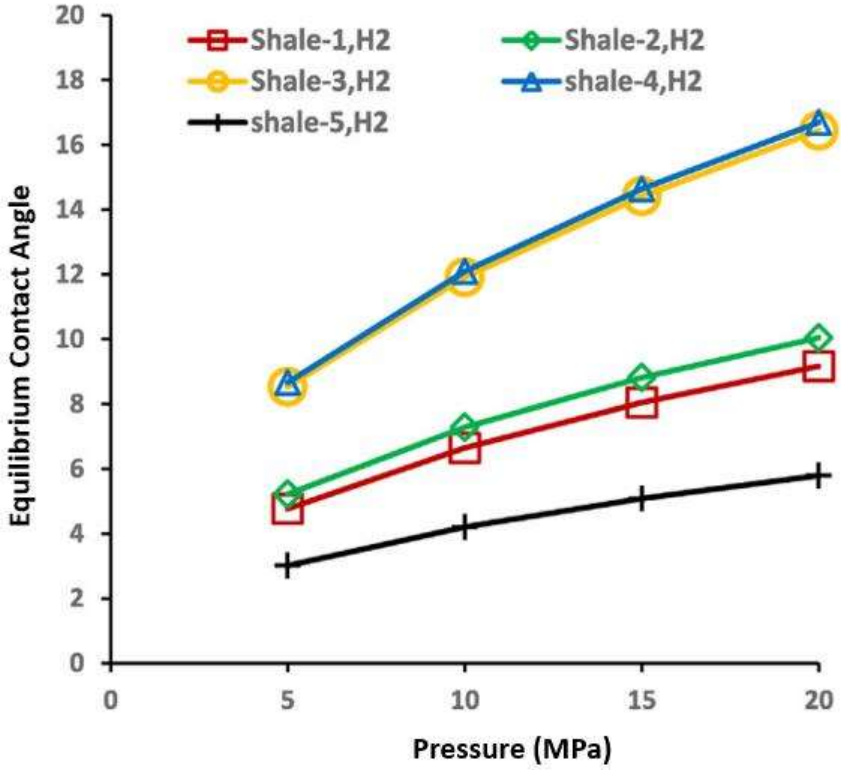

Fig. 13. Effect of pressure on the wettability of H_2/brine/shale [89].

Contrarily, Al-Mukainah et al. [58] noted that the CA of H_2/brine on shale decreases with an increase in pressure. The authors attributed the deviation from previous studies to the ultra-low density of H_2 gas at the pressure studied (1,000 psi). It is worth noting that an improved form of the sessile drop technique was used by the authors compared to other reported studies where the tilted plate method was used. It is therefore expected that the adopted methodology will promote contact angle decrease with increasing pressure as a single pendant was used by constantly compressing the pendant with increasing H_2 gas pressure. Whereas, the existing tilted plate method procedure involves an initial injection of H_2 gas at a set pressure before releasing the drop. Hashemi et al. [82] reported that the H_2/brine/rock contact angle is not influenced by the presence of pressure. Similarly, Higgs et al. [56] observed no correlation between the CA of H_2-brine-rock and pressure at constant temperature. This was ascribed to

546 the low solubility of hydrogen in water. More studies are required to elucidate the effect of
547 pressure on the wettability of H_2-Brine-rock systems.

548 **4.3 Effect of Temperature**

549 At high temperatures, the kinetic energy of H_2 gas increases. High collision and accelerated
550 diffusion occur while the molecular cohesive energy of the H_2 gas reduces. Consequently, the
551 molecular interaction between H_2 gas and the rock surface of the geologic medium reduces.
552 Zeng et al. [83] recorded an increase in the disjoining pressure of the calcite surface with an
553 increase in the temperature of the system via geochemical modelling of the rock surface.
554 Resultantly, a decrease in the contact angle and an increase in the hydrophilicity of the H_2
555 /brine/rock system was observed. Ali et al. [90] studied the wetting property of the
556 H_2/brine/rock system and observed that an increase in the temperature of the system resulted
557 in the reduction of the contact angle. At a fixed pressure of 15 MPa, the contact angle of the
558 mica/H_2/brine was recorded as $\theta_a = 53.1°$ and $\theta_r = 47.3°$ at 35 ℃, while $\theta_a = 35.4°$ and $\theta_r =$
559 $29.2°$ at 70 ℃, respectively (see **Figure 14**). Hosseini et al. [84] observed that an increase in
560 temperature reduced the water contact angle on H_2 /brine/carbonate surface. At 15 MPa, the
561 advancing CA decreased from $\theta_a = 80.35°$ at 25 ℃ to $\theta_a = 57.85°$ at 80 ℃ while the receding
562 CA decreased from $\theta_r = 76.6°$ at 25 ℃ to $\theta_r = 53.15°$ at 80 ℃.

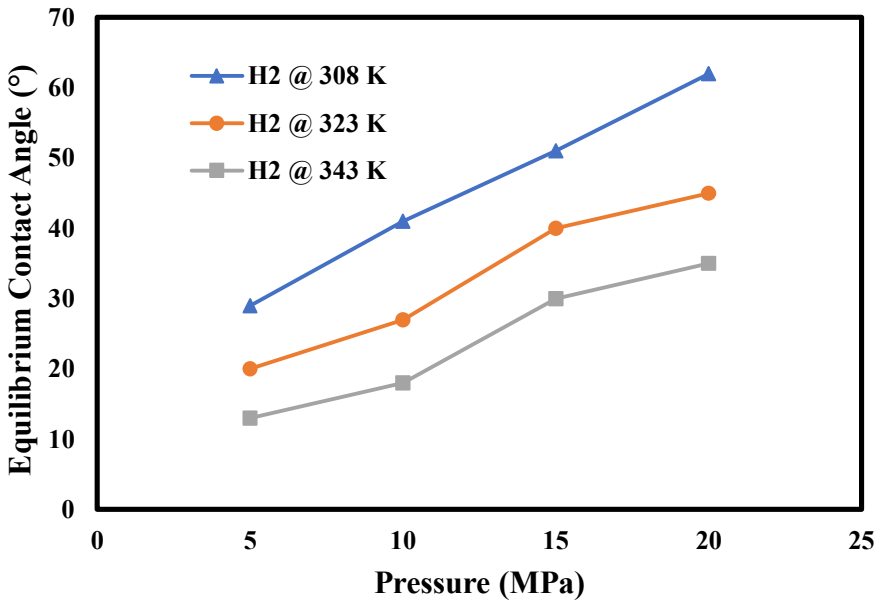

563

564 **Fig. 14.** Effect of temperature and pressure on the contact angle of H_2/brine/mica. Adapted
565 from [77].

Hosseini et al. [91] noted that the brine wettability of basalt increased water contact angle with an increase in temperature. For example, at 5 MPa, as $\theta_a = 32.29°$ at 35 ℃, while $\theta_a = 47.86°$ at 70 ℃. This was attributed to the breakage of hydrogen bond between the water molecule and silanol group of silica rich basaltic rock, thereby decreasing the hydrophilicity. Similarly, Iglauer et al. [87] discovered that an increase in temperature resulted in an increase in the contact angle for the H_2/brine/quartz system. The authors explained this phenomenon by postulating that as temperature increased, there was a higher probability of breaking hydrogen bonds between water molecules and silanol groups on the quartz surface. This led to a decrease in the concentration of surface hydrogen bonds, thereby reducing the hydrophilicity of the quartz and increasing the hydrogen wettability. At a pressure of 10 MPa, the contact angle increased from 12.3° at 23 ℃ to 33.7° at 70 ℃, providing evidence for the relationship between temperature and hydrogen wettability.

4.4 Effect of organic acid

The evolution of hydrocarbon from biological materials in hydrocarbon reservoirs implies that there is a tendency for trace amounts of organic acids (OA) to be present in depleted hydrocarbon reservoirs [37]. Hence, to mimic real reservoir conditions, the impact of OA concentration on the wettability of the H_2 /brine/rock has been investigated to understand UHS trapping and containment security. The presence of organic acid (even in minute quantity) increases the hydrophobicity due to adsorption at the rock interface and causes the de-wetting of the rock surface [87]. The de-wetting of rock surfaces has a significant impact on the trapping potential and containment safety of hydrogen in the geologic medium. Hosseini et al. [91] observed a reduction in water wettability when the OA concentration is increased. This was attributed to OA adsorption on the surface of the basaltic rock. Similarly, Ali et al. [86] studied the H_2 – rock wettability using a quartz sandstone substrate. Three organic acids namely lauric acid, hexanoic acid, and lignoceric acids were used to mimic the presence of hydrocarbons typical of real reservoir conditions. An increase in hexanoic acid concentration from $10^{-9}M$ to $10^{-2}M$ at a fixed temperature 323 $°K$ and pressure 25 MPa caused a wettability alteration to an intermediate wetting condition ($\theta_a = 68.2°$, $\theta_r = 61.5°$) from a water wetting condition ($\theta_a = 42.9°$, $\theta_r = 38.6°$). Similarly, $10^{-2}M$ lignoceric acid concentration increased the CA of quartz/H_2/brine to intermediate wetting condition ($\theta_a = 91.3°$, $\theta_r = 82.7°$) from water wetting condition ($\theta_a = 55.6°$, $\theta_r = 55.6°$).

As shown in **Figure 15**, Ali et al. [88] investigated the role of organic acid structures on the wetting characteristics of mica as a representative of the caprock. At 25 MPa pressure and $10^{-2}M$ fixed concentration for hexanoic acid, lauric acid, and lignoceric acid, the contact angle changed to 80.3°, 89.2°, and 106.2°, respectively. Furthermore, at a fixed concentration of organic acid, the molecular structure of organic acid plays a crucial role in determining the degree of change of the wetting condition. Increasing the alkyl chain length (number of carbon atoms) causes an increase in the quartz/H_2/brine contact angle. Similar result was reported in the case of Indiana limestone rock [92]. This is because the increasing concentration of the alkyl chain causes an increase in the standard energy of adsorption and consequently, stronger interaction with the mica substrate. Hence, the presence of organic acid in geological formations at high pressure implies that there is a possibility for the structural trapping capacity of the caprock to fail and a high possibility for H_2 gas leakage.

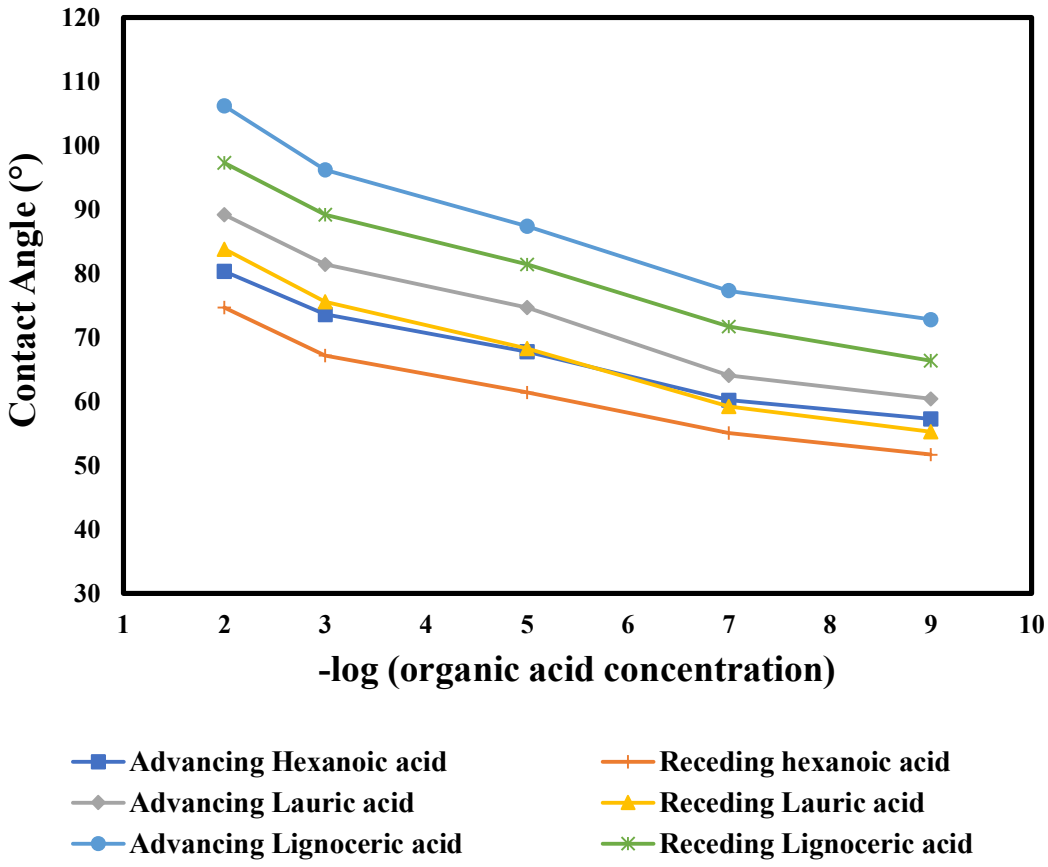

Fig. 15. Comparison of H_2 /brine/rock wettability for mica and quartz surface at different temperature and pressure conditions. Adapted from [88].

4.5 Effect of rock mineralogy

The mineralogy of rock also plays a distinct role in the wettability of rock and hence, the trapping potential of the geologic medium. Ali et al. [88] studied the H_2 /brine/rock wettability of quartz and mica under similar organic acid concentrations, temperatures, and pressure conditions. At $10^{-3}M$ lignoceric acid concentration, the advancing contact angle for quartz/ H_2 /brine is recorded as 51.3°, 69.2°, and 84.6° for 0.1, 15, and 25 MPa, respectively. On the other hand, at similar conditions, the advancing contact angle for mica/ H_2 /brine is recorded as 60.7°, 85.7°, and 96.2° for 0.1, 15, and 25 MPa, respectively. The higher contact angle recorded for mica compared to quartz was adduced to the presence of more silanol groups on the quartz surface which presents it with more hydrophilic sites and enabled maximum interaction with the H_2 moieties.

Al-Mukainah et al. [58] evaluated the potential of UHS in shale formations. Two shale rocks namely Eagle-ford shale and Wolf-camp shale rocks have total organic carbon (TOC) of 3.83% and 0.30%, respectively. At low pressures, the Eagle-ford shale was intermediately wet. On the other hand, the Wolf-camp shale was weakly water-wet throughout the pressure range studied. This was attributed to the increase in the TOC content of shale which decreases the water-wettability of the H_2-brine-rock system. Al-Yaseri et al. [89] studied the effect of shale TOC on the wettability of the H_2 /brine system. They noted that shale with higher TOC recorded high contact angles due to its high hydrophobicity. Hosseini et al. [93] observed a similar trend for shale rock samples with different TOC concentrations. The authors noted that when the TOC of the shale rock sample was increased from 0.09 wt.% to 14 wt.% (at 15 MPa, and 50 ℃), the receding contact angle of H_2 /brine/rock increased from 31.77° to 82.4°, indicating a decrease in the water-wetness of the shale rock. It was inferred that the increase in the TOC cause an increase in the hydrophobicity of the shale rocks and consequently a decrease in the water-wetness of the shale rock. Furthermore, the authors noted that shale samples with higher amounts of calcite and clay tend to have more hydrogen wettability (i.e., high water contact angle and low water-wetness). On the other hand, evaporite rock sample with high content of gypsum tends to be water wet.

Esfandyari et al. [60] investigated the H_2 /brine/rock wettability of different rocks under varying salinities, temperatures, pressures, and OA concentrations. They observed that the mineralogy of the reservoir rock system has a distinct effect on the CA values of H_2 /brine/rock. At a temperature of 80 ℃ and pressure of 10 bar, the CA of H_2 /brine/rock for gypsum, quartz, anhydrite, calcite, shale, dolomite, granite, and basalt are recorded as 48°, 45°, 40°, 40°, 39°,

37°, 27°, 21°, respectively. However, the mechanism of the influence of rock mineralogy on the wettability of the system was not elucidated. Likewise, Hou et al. [85] measured the H_2 /brine/rock wettability of three different rocks namely sandstone, shale coal, and carbonate rocks. At 5 wt.% NaCl concentration, the average contact angle was recorded as 42.3°, 48.4°, and 67.2° for sandstone, shale coal, and carbonate rocks, respectively.

Al-Yaseri et al. [94] inferred the H_2 /brine/rock wettability of different clays (kaolinite, illite, and montmorillonite) using empirical correlations on measurement of other similar gases (CO_2, N_2, He, and Ar) conducted at subsurface conditions. All evaluated clays were found to strongly exemplify water-wetting behavior. The water-wetness of the clay surface in the presence of hydrogen is in the order of kaolinite > illite > Montmorillonite. The lower water contact angle (i.e., high water wetness) of kaolinite clay surface was ascribed to the hydrophilic surface of kaolinite clay characterized by a 1:1 tetrahedral siloxane (T-sheet) and octahedral hydroxide surface (O-sheet). Contrariwise, illite and montmorillonite are 2:1 clay whose O-sheets are placed in-between two T-sheets. The contact angle result depicts that the structural and residual trapping of hydrogen would be highly favoured on a clay surface.

4.6 Effect of Cushion gas

The injection of cushion gas as a buffer to improve the storage and withdrawal efficiency of H_2 necessitates that the impact of the cushion gas on the wettability of the process be studied. Nevertheless, only a handful of experimental studies on mixtures of H_2 with cushion gas exist in the literature. For example, Mirchi et al. [17] performed contact angle experiments using the captive bubble method for H_2/CH_4 mixtures on oil-wet sandstone and limestone at 1000 psi for three different temperatures (22, 40, and 60 ℃) and 2 wt.% salinity. The contact angle of the oil-wet rock surface was recorded as 130.4° and 136.2°. On the other hand, the presence of the gas mixtures altered the wettability of the rock surfactant to weakly water-wetting conditions of 59.72° and 71°. Their findings further posited CH_4 gas as a promising cushion gas option in a depleted oil and gas reservoir [17].

In a similar manner, Hashemi et al. [95] utilized a captive bubble setup to measure the contact angle of H_2-CH_4 Bentheimer sandstone under UHS conditions, including pressures, temperatures and varying salinities. Their findings indicated a strongly water-wet condition with contact angles between 25 to 45°. They also revealed that the measured contact angle remained unaffected by the investigated reservoir temperature, pressure, and salinity. A recent

study by Alanazi et al. [72] used the tilted plate method to investigate the impact of CH_4-cushion gas on substrates derived from organic-oil-rich shale source rocks from Jordan. The researchers examined the effect of gas type (pure CH_4, pure H_2, and H_2-CH_4 mixtures) and pressure on geo-storage conditions by measuring the contact angle at 50 ℃ under various pressures and salinities. The results indicated that the contact angle levels for rock/CH_4/brine were greater than rock/H_2/brine, while the H_2-CH_4/brine mixture contact angles were intermediate between those for pure gases.

From the above cushion gas type, it can be observed that only CH_4 has been experimentally investigated with respect to H_2-CH_4 mixtures on wettability. Hence more studies on other cushion gas types such as CO_2 and N_2 are highly encouraged to fully comprehend the general behaviour during hydrogen injection. Moreover, the choice of cushion gas is determined by various factors. One such factor is the gas wettability, which is higher in N_2 and CO_2 [90,96,97], making them easier to separate during production cycles. Similarly, cost [98,99], physical properties [100], and geological parameters such as reservoir depth, trap shape, and permeability [69] are other considerations that need to be considered during cushion gas selection.

694 **Table 3.** Wettability studies of pure (H_2/brine/rock) and mixed (H_2-CH_4/brine/rock) systems relevant for UHS.

Reference	Methodology	Substrate	Organic acid	Gas	Salinity	Temperature	Pressure	Significant findings
Iglauer et al. [87]	Tilted plate goniometry	Quartz (Sandstone)	Stearic acid	H_2	10 wt.% NaCl	23 – 70 °C	0.1 – 25 MPa	• Contact angle of the system increased as a function of pressure, temperature, and organic acid concentration.
Hashemi et al. [82]	Captive bubble	Bentheimer and Berea Sandstone	–	H_2	0 wt.% NaCl 0.5 wt.% NaCl, 5.0 wt.% NaCl SW 3.677 wt.%	20, 30, 40, 50 °C	20, 50, 70, 100 bars	• H_2-brine-rock demonstrated a strongly water-wetting condition. • Variation in rock type, salinity, temperature, and pressure does not have a significant effect on the wetting property of the system.
Ali et al. [86]	Tilted plate goniometry	Quartz (Sandstone)	Hexanoic acid, Lauric acid, Lignoceric acid	H_2	10 wt.% NaCl	50 °C	0.1, 15, 25 MPa	• Quartz surface exemplified strongly water-wet to

								intermediate-wetting conditions. • Contact angle also increased with increasing pressure.
Ali et al. [88]	Tilted plate goniometry	Mica	Hexanoic acid, Lauric acid, Lignoceric acid	H_2	10 wt.% NaCl	50 °C	0.1, 15, 25 MPa	• H_2–rock wettability increased with an increase in the concentration of organic acids and length of the alkyl group. • Increase in pressure increases the CA of the H_2-brine-rock interface.
Ali et al. [90]	Tilted plate goniometry	Mica	Stearic acid	H_2	10 wt.% NaCl	35– 70 °C	0.1 – 25 MPa	• Rock/H_2/brine wettability decreases with increasing temperature. • Contrariwise, H_2 /brine wettability increases with increasing pressure

								and organic acid concentration.
Higgs et al. [56]	Captive bubble, *in-situ* micro-CT scanning	Quartz, Bentheimer, Berea	–	H_2	0.1, 0.2, and 0.5 wt.% NaCl 16.7 wt.% KI	25 °C	0.69 – 20.68 MPa	• H_2-brine-rock exhibited a water-wetting condition. • No correlation was found between the CA of the rock-H_2 system with salinity and pressure.
Al-Yaseri and Jha [96]	Tilted plate goniometry	Basalt	–	H_2 CO_2, N_2, and He.	4.0 wt.% NaCl, 4.0 wt.% $CaCl_2$, 1 wt.% KCl, 1 wt.% $MgCl_2$	50 °C	5, 10, 15, and 20 MPa	• The basalt exhibited a strongly water-wetting state. • Besides, the contact angle of rock-H_2 increases with pressure.
Al-Yaseri et al. [94]	Tilted plate goniometry	Kaolinite, Illite and Montmorillonite clays.	–	H_2, CO_2, Ar, N_2, and He.	Brine, 20 NaCl, and 1 KCl	60 °C	725 – 2900 psi	• A strongly water-wet condition was reported. • The predicted contact angle increases with

								pressure for all the tested clay samples.
Al-Mukainah et al. [58]	Sessile drop	Shale (Wolf camp and Eagle ford)	–	H_2	10 wt.% NaCl	50 °C	14.7 – 1000 psi	• The contact angle increases as a function of the TOC content of the shale rock. • Contact angle also decreased with increasing pressure.
Hosseini et al. [91]	Tilted plate goniometry	Basalt	Stearic acid	H_2	1.05 M brine (0.864 mol NaCl & 0.136 mol KCl)	35 – 70 °C	5 – 20 MPa	• At lower pressures (5 and 10 MPa), the basalt-H_2-rock system exhibited a strongly water-wetting behaviour. • Nonetheless, at higher pressures (15 and 20 MPa), the wettability of the system changed to a weakly water-wetting condition.

								• Increase in the organic acid concentration and temperature changed the wettability to an intermediate wetting condition.
Hosseini et al. [84]	Tilted plate goniometry	Calcite	Stearic acid	H_2	0 – 4.95 mol/kg	25 – 80 °C	0.1 – 20 MPa	• An increase in the pressure of the H_2-bine-calcite rock system changed the wettability of the rock surface from strongly water-wet to intermediate-wet. • Similar behaviour was observed for an increase in salinity and organic acid concentration. However, an opposite trend was observed for an increase in temperature.

Hosseini et al. [93]	Tilted plate goniometry	Shale, evaporite, and oil shale	Stearic acid	H_2	1.05 M brine (0.864 mol NaCl & 0.136 mol KCl)	25 – 80 °C	0.1, 5, 10, 20 MPa	• The outcome of the study revealed that an increase in the TOC of shale, pressure, and organic acid concentration causes an increase in the contact angles of the H_2-brine-rock system. • A reverse trend was observed for an increase in temperature conditions.
Esfandyari et al. [60]	Captive drop technique	Calcite, dolomite, quartz, shale, anhydrite, gypsum, granite, and basalt	Stearic acid	H_2	Distilled water, Formation brine	20 – 80 °C	10 – 100 bars	• The contact angles of granite, quartz, basalt, and gypsum demonstrates a water-wetting behaviour of H_2, indicative of good storage capabilities. • On the other hand, the surface wettability of calcite, shale, dolomite,

								and anhydrite exemplified weakly water-wetting or neutral wetting behaviour.
Sedev et al. [101]	Tilted drop method	Bituminous coal	–	H_2	2.0 wt.% NaCl	25, 50, 70 °C	5 – 90 bars	• The contact angle of the H_2-bine-coal system is weakly water-wet throughout the temperature and pressure conditions studied.
Hou et al. [85]	Sessile drop	Aged carbonate, sandstone, and shale samples	n-decane/stearic acid solutions	H_2	0.1 to 5 brine solutions of NaCl, CaCl, Na_2SO_4, $MgCl_2$, and $MgSO_4$	25 – 70 °C	14 – 4351 psi	• Strongly water-wet to intermediate-wet conditions were observed with ionic changes. • Overall, the contact angles increased with decreasing temperature but were found to increase with the increase of ions

								concentration, and pressure, respectively. • Divalent ions had a significant impact on the H_2 wettability alteration than monovalent ions.
Hashemi et al. [95]	Captive bubble	Bentheimer	–	H_2 CH_4 and H_2–CH_4 mixture	Pure water, 0.5 wt.% NaCl, 5 wt.% NaCl	30, 50 °C	20, 50, 70, 100 bars	• The H_2-brine-rock demonstrated a water-wetting behaviour. • Besides, the contact angle of H_2 and H_2–CH_4 mixtures does not change with salinity, temperature, and gas composition.
Mirchi et al. [17]	Captive-Bubble	Oil-aged sandstone and limestone	–	H_2, CH_4 and H_2–CH_4 mixture	Brine, 2 NaCl	22, 40, 60 °C	1000 psi	• Weakly water-wet conditions were observed, with the static contact angle higher for pure CH_4 gas than H_2–CH_4 mixtures.

								• Furthermore, the reported contact angle behaviour was independent of temperature increase.
Alanazi et al. [71]	Tilted plate	Jordanian organic oil shale samples	–	H_2, CH_4 and H_2–CH_4 mixture	Brine, 2 NaCl Brine, 1 KCl	50 °C	0.1 to 1600 psi	• The organic-rich shale demonstrates a weakly water-wet to weakly H_2-wetting property especially in the mixing zone. • Similarly, the dynamic contact angles increased with pressure at a constant temperature.
Jangda et al. [102]	Micro CT scanner	Bentheimer Sandstone	–	H_2	Brine	50 °C	100 bars	• After pore scale displacement processes, the porous sandstone rock was found to be non-wetting to H_2 and wetting to brine.

								• Contact angles of 53° and 54° were reported for the rock sample in non-H_2-equilibrated brine and H_2-equilibrated brine, respectively.
Aghaei et al. [103]	Captive bubble method	Calcite, Dolomite, Anhydrite	–	H_2	Brine	30 °C, 75 °C	3.44, 10.34, and 17.23 MPa	• The carbonate rocks remain strongly water-wet (contact angles < 30°) for all conditions studied. • Moreover, temperature and pressure have no significant effect on the contact angle of the representative host-rock and caprock.

695 H_2O = Pure water, KI = Potassium Iodide, KCl = Potassium chloride, NaCl = Sodium chloride, CaCl = Calcium chloride, Na_2SO_4 = Sodium
696 sulfate, $MgCl_2$ = Magnesium chloride, and $MgSO_4$ = Magnesium sulfate.

5. Adsorption

Adsorption of hydrogen is another important parameter that plays a critical role in fluid-rock interaction and hence, is considered very crucial to the success of underground hydrogen storage. Previous studies of gas adsorption processes have investigated N_2, CO_2, and CH_4 adsorption on reservoir rock, shale, and coal. However, only a handful of research contributions exist on H_2 adsorption due to the complexity involved in handling H_2 gases. The adsorption of H_2 on reservoir rock systems is controlled intrinsically, based on the van der Waal's bonding the gas exhibits on the host rock system. Hence, it has lower/weaker adsorption compared to other gases (e.g., CO_2, CH_4) on a reservoir rock system due to the low hydrogen density. The adsorption of H_2 on porous media is dependent on several factors; these include temperature, pressure, organic acid content, mineral content, and surface chemistry.

Samara et al. [104] studied the adsorption behavior of H_2 and CO_2 on Jordanian shale rocks. Mineralogical characterization of the rock depicts that it predominantly contains calcite and other minerals such as quartz, dolomite, and pyrite. The adsorption of H_2 and CO_2 gas at 50 bars measured from a magnetic suspension balance was recorded as 0.015 wt.% and 0.83 wt.%, respectively. The higher adsorption of CO_2 on the shale rock surface compared to H_2 gas is attributed to the composition of the shale, with calcite as the dominant mineral which provides a higher affinity for CO_2 gas due to higher electronegativity difference. Also, the dissolution of CO_2 on kerogen increases the quantity of CO_2 trapped on the surface of the shale. Conversely, H_2 gas has a quadrupole moment which is one order of magnitude lower than CO_2, hence recording lower adsorption due to the weaker interaction between H_2 with calcite, and H_2 with kerogen.

Additionally, the storage of hydrogen in shale is a function of its aromaticity. Raza et al. [105] evaluated the effect of kerogen content and maturity on H_2, CO_2, and CH_4 storage potential in underground reservoirs via molecular dynamics simulation. The adsorption process was conducted at a broad range of pressure (2.75 to 20 MPa) and temperature (50 – 150 ℃) regimes. To portray the impact of maturity, four kerogen structures were used, namely type II-A, II-B, II-C, II-D. The carbon content and hence the maturity of the kerogens are in the order of II-A < II-B < II-C < II-D. At a given temperature and pressure, the computational result indicates that the sorption of the gases increases with an increase in kerogen maturity and carbon content. For example, the adsorption of H_2 increased from 2.4 to 3.0 mmol/g for type II-A (40% carbon

content) and type II-D (80% carbon content), respectively. This was ascribed to the increasing heteroatomic functional groups of the kerogen and the effective volume of the pores.

Furthermore, Abid et al. [106] investigated the effect of organic acid (humic acid) on the adsorption behaviour of H_2 and CH_4 on shale rock via a PCT pro adsorption analyzer. The experiment was carried out to depict real geo-storage conditions. Experimental results revealed high adsorption of H_2 gas on shale contaminated with humic acid compared to the raw shale sample. At 30 ℃ and 42.7 bar, the adsorption of raw shale and shale with humic acid (shale-HA) is recorded as 0.056 mol/kg and 0.3 mol/kg, respectively (see **Figure 16**). The high adsorption witnessed by shale-HA was adduced to the increase in total organic content (TOC) caused by the presence of humic acid, higher micropore content and increased surface area.

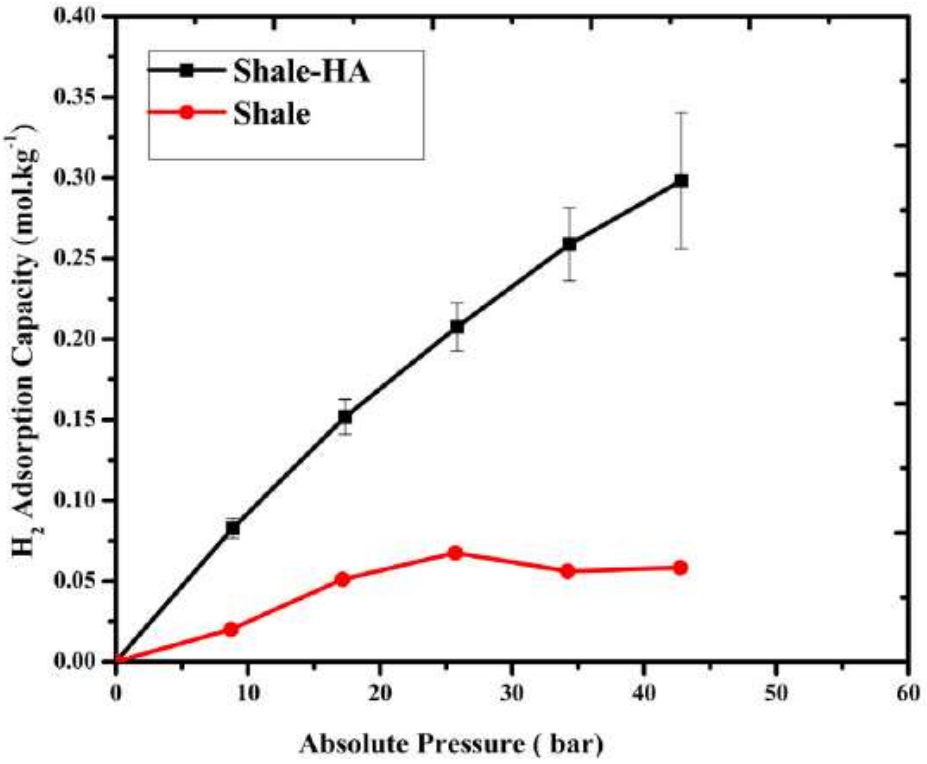

Fig. 16. Adsorption behaviour of H_2 gas on raw shale and shale aged with humic acid [106].

Apart from shale, hydrogen storage has also been explored in coal seams due to its large surface area and its previously established capacity for the sequestration of carbon dioxide [107,108]. Iglauer et al. [109] experimentally determined the feasibility of storing hydrogen in coal seams. The H_2 adsorption experiment on sub-bituminous coal was performed using a PCTpro adsorption analyzer and compared to CO_2. Notably, the H_2 adsorption increases drastically as

745 a function of pressure until it reaches a plateau as depicted in **Figure 17**. Meanwhile, H_2
746 adsorption decreases as a function of temperature albeit infinitesimally. The maximum H_2
747 adsorption on the monolayer of the coal was recorded as 0.60183 moles of H_2/kg of coal at
748 14.3207 MPa. Similarly, Keshavarz et al. [110] evaluated the adsorption behaviour of H_2 on
749 coal seam and noted that the adsorption of H_2 decreases with an increase in temperature.
750 Additionally, H_2 adsorption on coal is a function of the aromatic content of coal. Arif et al.
751 [111] experimentally analysed hydrogen storage as a function of coal ranking at varying
752 temperatures and pressures using anthracite, bituminous, and sub-bituminous coals with a
753 vitrinite content of 78.9, 58.7, and 33.3, respectively. At a particular temperature and pressure,
754 the highest adsorption was recorded on high-rank coal (see **Figure 18**). This implies anthracite
755 coal with relatively higher aromatic and lower oxygen content demonstrated the highest
756 adsorption compared to bituminous and sub-bituminous coals (anthracite > bituminous > sub-
757 bituminous).

758

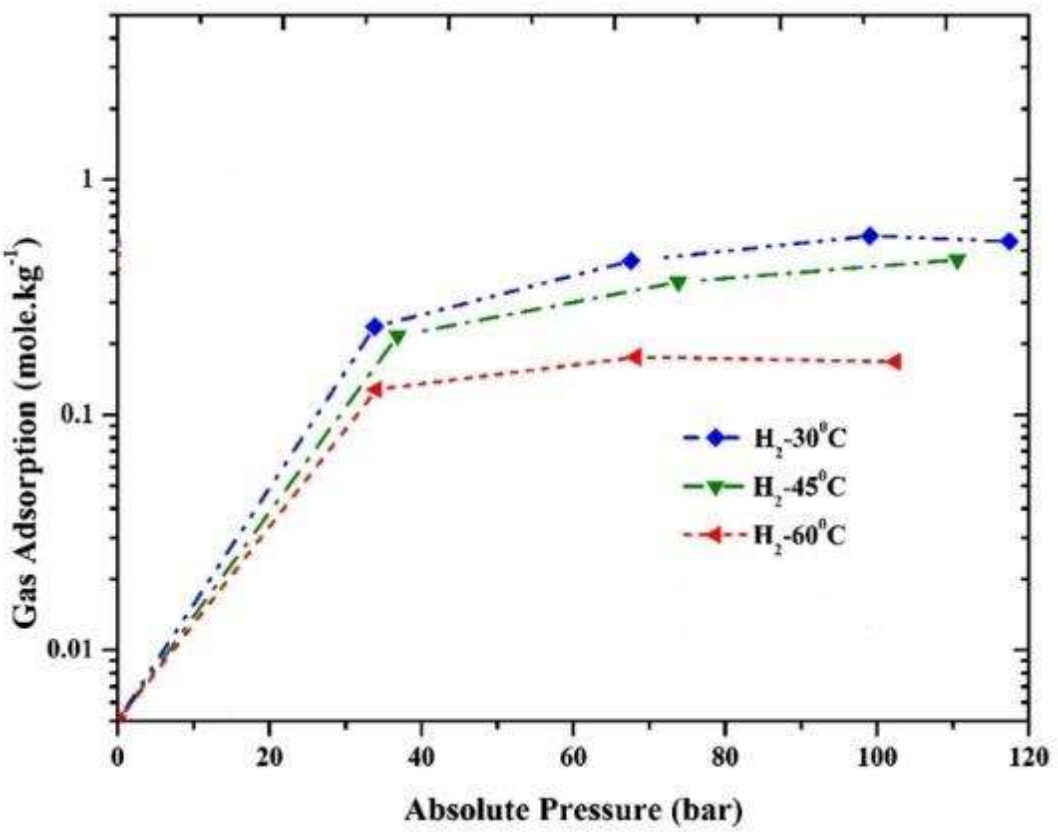

759

760 **Fig. 17.** Adsorption of hydrogen on sub-bituminous coal. Modified from [109]

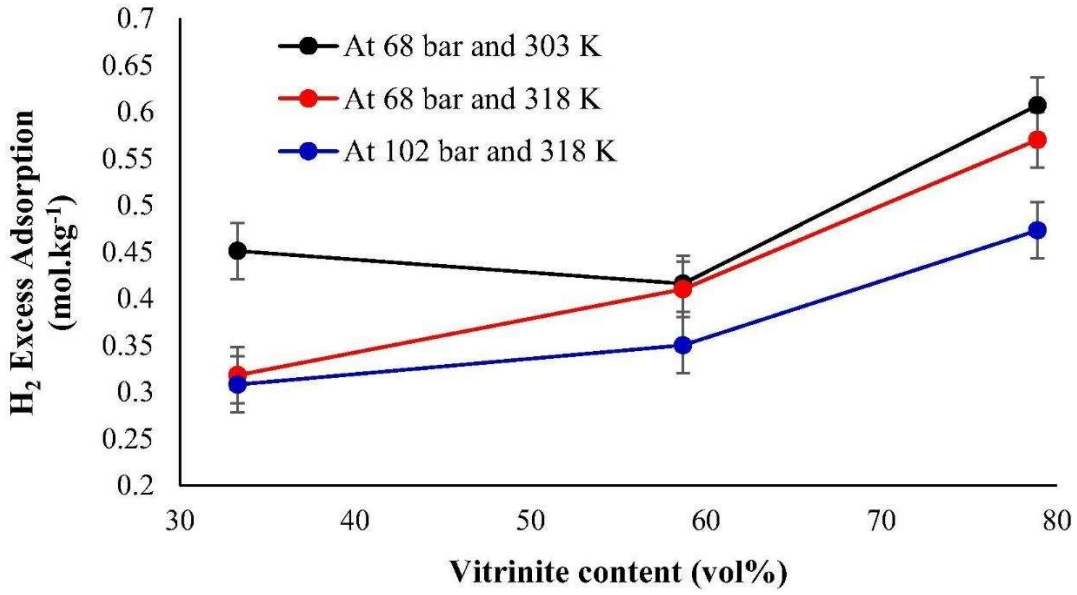

761

762 **Fig. 18.** H_2 adsorption versus vitrinite content of coals [111].

763 Underground hydrogen storage has also been conducted in representative reservoir rock
764 systems. Carchini et al. [112] assessed the feasibility of UHS in depleted gas reservoirs via
765 experimental and molecular modelling approaches. The adsorption/desorption experimental
766 analysis was conducted using a Rubotherm magnetic suspension balance on carbonates and
767 sandstone rocks. At a moderate temperature of 50 ℃ and pressure of 20 bar, no adsorption of
768 H_2 gas on calcite was recorded while a negligible quantity (0.06 mg/g) of H_2 gas adsorption on
769 dolomite was achieved. Likewise, no uptake of H_2 gas was recorded on Berea and Scioto
770 sandstone, indicative of low and high clay-rich sandstone, respectively. Moreover, a further
771 increase in the temperature to 100 ℃ yielded no considerable result. The low physisorption of
772 H_2 gas in the pore network of the reservoir rock system was adduced to a lower kinetic diameter
773 of hydrogen.

774 López-Chávez et al. [113] conducted a modelling and simulation study of the adsorption
775 behaviour of H_2 on calcite rock for geo-storage. Firstly, they described and optimized the
776 calcite rock model using density function theory (DFT). Moreover, the naturally fractured rock
777 was characterized using DFT to obtain the Mulliken population analysis, electronic,
778 thermodynamic, structural, and thermodynamic properties. Lastly, molecular dynamics
779 simulation process was carried out to simulate the adsorption process and to estimate the H_2
780 adsorption on the surface of the calcite rock. The simulation process revealed that 0.42 mass
781 percent of H_2 is adsorbed on the surface of calcite rock.

782 The adsorption/desorption behaviours of H_2 on clay structures have also been studied. It is
783 crucial to understand the integrity of the caprock which is typically made up of a clay structure.
784 Wolff-Boenisch et al. [114] evaluated the adsorption behaviour of hydrogen on
785 montmorillonite clay. As can be seen in **Figure 19**, the adsorption process was fitted using
786 Langmuir and Freundlich isotherm. At 30 ℃, 0.18 mol/kg of H_2 was adsorbed on the clay
787 indicative of low adsorption. This was attributed to the lack of dipole moment on H_2 symmetry
788 to enable intermolecular bonding with the clay structure. Besides, desorption of the H_2 gas on
789 the montmorillonite clay was observed with increasing temperature due to an increase in kinetic
790 energy. Conspicuously, the gas prefers to stay in the gas phase rather than adsorb on the solid
791 phase of the clay structure. Hence, the authors recommended the injection of H_2 deeper into
792 the formation because the temperature and pressure reduce hydrogen loss via adsorption, and
793 this enhances higher storage volumes of H_2 gas.

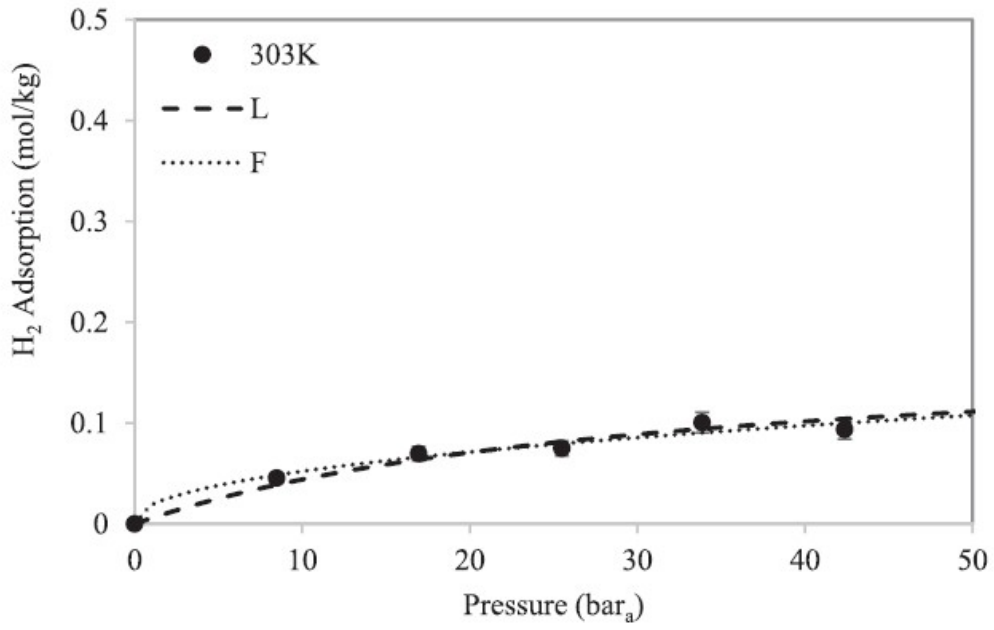

794

795 **Fig. 19.** Adsorption of hydrogen on clay [114].

796 Likewise, Bardelli et al. [115] determined hydrogen adsorption on clay-rich rock formation.
797 The experiment was carried out on raw clay samples (COX_{raw}) and pure clay sample
798 (COX_{pure}) at pressures up to 80 bars and temperature of up to 90 ℃. The sorption experiment
799 at the highest temperature indicates that the hydrogen uptake reaches a plateau at around 40 –
800 60 bars and the adsorption for COX_{raw} and COX_{pure} was estimated as 0.12 ± 0.01 wt.% and
801 0.2 ± 0.02 wt.%, respectively. Moreover, Didier et al. [116] evaluated H_2 adsorption on similar

rock samples at the same temperature (90 °C) but a lower pressure of 0.45 bar. H_2 sorption of 0.05 wt.% and 0.06 wt.% was recorded for COX_{raw} and COX_{pure} samples, respectively.

The low adsorption behaviour of H_2 gas on conventional and unconventional reservoir rock systems is indicative of the good potential for storage and subsequent withdrawal from the pore networks of their geologic structure. However, only a few studies exist on the adsorption behaviour of H_2 gas on reservoir rock systems. Most of the existing H_2 adsorption studies were carried out on representative reservoir rock systems. Extended studies on the adsorption property of H_2 gas on carbonate, sandstone, and dolomite rocks at typical reservoir conditions are desired. Moreover, most experimental studies of H_2 adsorption at high pressures are conducted over a short time due to volatility issues. A systemic approach that allows for long-term evaluation of H_2 storage at typical geo-storage conditions is required to ascertain real field conditions. Furthermore, cushion gas has been suggested to act as a buffer during UHS. However, studies of the impact of cushion gas on the sorption behaviour of H_2 gas are lacking in the literature. Finally, the effect of fluid composition, pore structure, and pore geometry on H_2 adsorption behaviour on reservoir rocks remains obscure. This is required to fully understand the trapping mechanism of H_2 storage in reservoir rock systems.

6. Diffusion

Diffusion is a transport phenomenon that describes the spreading of fluids and particles through a medium. In fluid-fluid systems, diffusion is related to the transport of one fluid component through another fluid whereas in fluid-rock systems, diffusion can be used to describe the transport of fluids (such as gas) through a porous rock matrix. Diffusivity, on the other hand, is a physical quantity that describes the ability of a substance to diffuse through a medium.

Hydrogen diffusivity (D_{H_2}) – herein, refers to the ability of hydrogen molecules or atoms to move through a medium by diffusion. It is a measure of how quickly or slowly hydrogen can move through a material and is influenced by factors such as temperature, pressure, brine salinity, fluid type and the properties of the material or transport medium itself. Therefore, understanding D_{H_2} is important in hydrogen storage and transport through the porous media as it can be used to calculate the amount of H_2 lost [39]. The role of D_{H_2} with respect to UHS cannot be overemphasized as it is one of the key factors influencing the leakage tendency of H_2 in the overlying caprock during structural trapping.

Figure 20 illustrates the dependence of D_{H_2} on various temperatures, pressures, and fluid types. It can be observed that, for each hydrocarbon fluid type, D_{H_2} decreases with increasing temperature and pressure. For example, when the pressure increased from 0.53 MPa to 2.2 MPa at 323 K, D_{H_2} in C_4H_{10} decreased from 740×10^{-8} m^2/s to 250×10^{-8} m^2/s, whereas it decreased from 620×10^{-8} m^2/s to 220×10^{-8} m^2/s at 298 K. A similar trend is also observed for C_3H_8, C_2H_6, and CH_4 gases [52,117–119]. Additionally, the number of carbon atoms in the hydrocarbon fluid is inversely proportional to the value of D_{H_2}. This can be observed in the decrease of D_{H_2} values for CH_4, C_2H_6, C_3H_8, and C_4H_{10} at 323 K and 1.4 MPa, which were 650×10^{-8} m^2/s, 480×10^{-8} m^2/s, 390×10^{-8} m^2/s, and 350×10^{-8} m^2/s respectively [52,117].

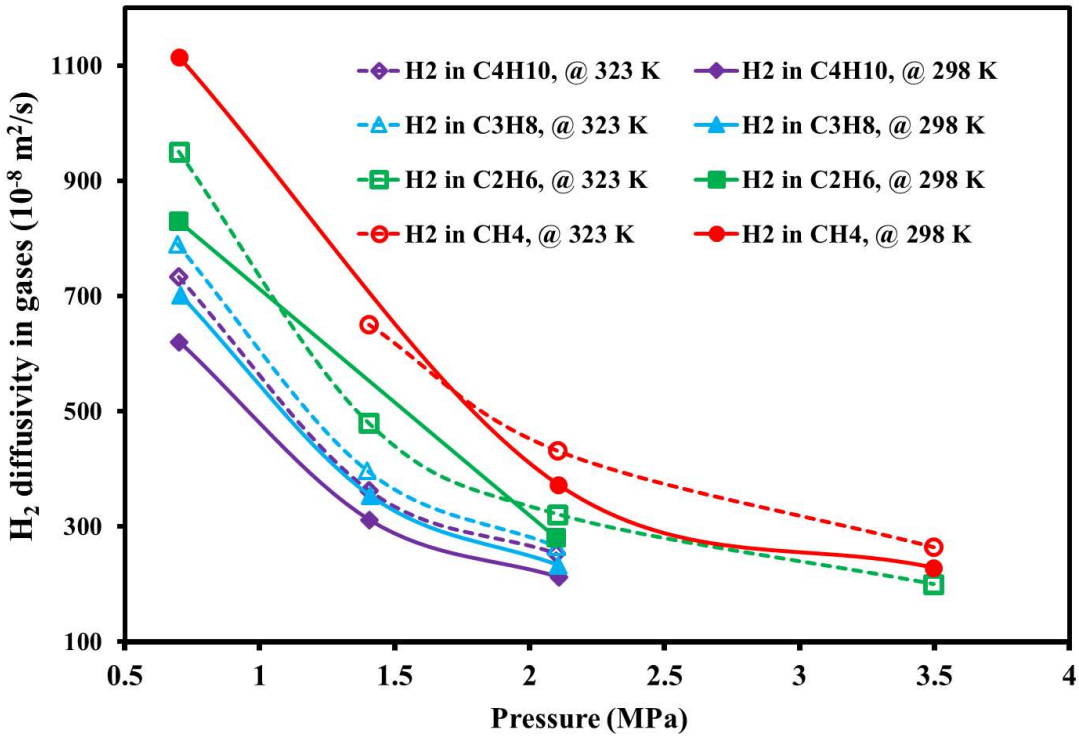

Fig. 20. H_2 diffusivity for hydrocarbon fluids as a function of temperature and pressure. Adapted from [52].

On the other hand, **Figure 21** illustrates D_{H_2} in water as a function of pressure and temperature. Unlike the case of hydrocarbon fluids, it can be observed that D_{H_2} increases with an increase in both temperature and pressure. For instance, at 25 MPa, as the temperature increased from 650 K to 970 K, D_{H_2} in water increased from 15.1×10^{-8} m^2/s to 219×10^{-8} m^2/s [119]. This phenomenon is attributed to the effect of temperature on molecular momentum, and

intermolecular forces, which ultimately influence diffusivity [120]. When both cases (i.e., **Figures 20** and **21**) are compared, it can be seen that hydrogen has a relatively high diffusion rate in water (or brine) compared to other gases. As a result, diffusion-induced hydrogen loss from aquifers is likely to be higher than in depleted oil and gas reservoirs where less residual brine is present. This, amongst many other factors, makes depleted gas reservoirs to be considered the most promising means for large-scale H_2 storage in porous media as the leakage potential is minimal [30,32]. However, only a 1% loss of injected H_2 via diffusion in aquifers has been reported after 15 years of simulation in a 7 m high reservoir with 20% porosity [121]. The reason for the difference in diffusion can be adduced to its small molecule size characteristics compared to other gases [118,119].

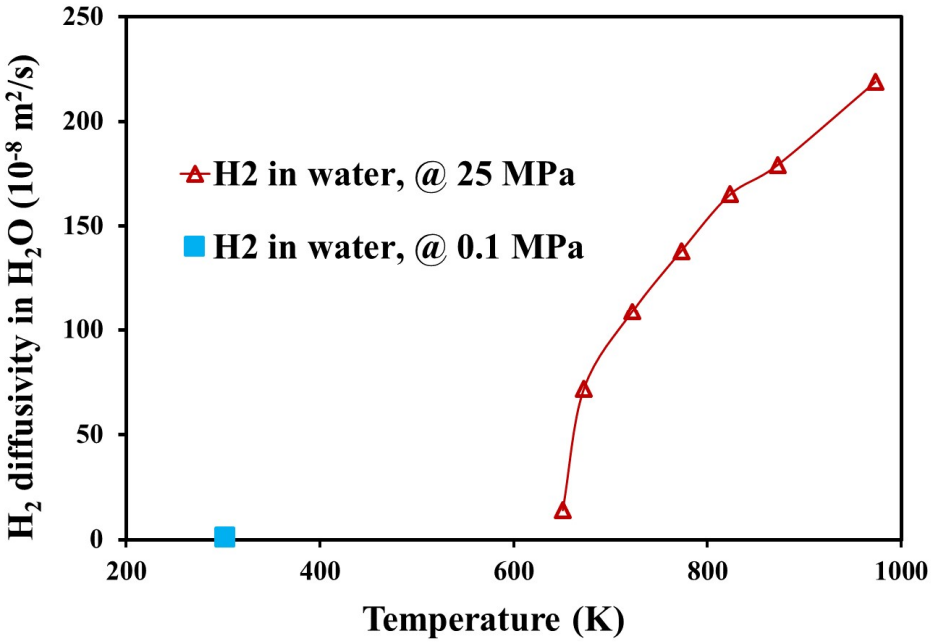

Fig. 21. H_2 diffusivity in water as a function of temperature and pressure. Adapted from [52].

D_{H_2} has also received significant attention from both experimental and simulation perspectives. In both cases, the available literature sources – experimental [122–128] and theoretical, via molecular dynamics simulation [118,119,129–131] have been limited to the case of H_2-pure water systems. Only, the recent study by van Rooijen et al. [39] made an effort to assess the self-diffusivity of H_2 in an aqueous solution at various pressures (1 – 1000 bar), temperatures (298 – 723 K) and brine molalities of 0 – 6 m NaCl/kg. As presented in **Figure 22(a)**, the self-diffusivities of H_2 show weak pressure dependence, which is consistent with the findings of Tsimpanogiannis et al. [132]. However, at a higher temperature of 723 K, the effect becomes

more noticeable. This was attributed to the increase in compressibility of the solution with increasing pressure of the H_2 gas.

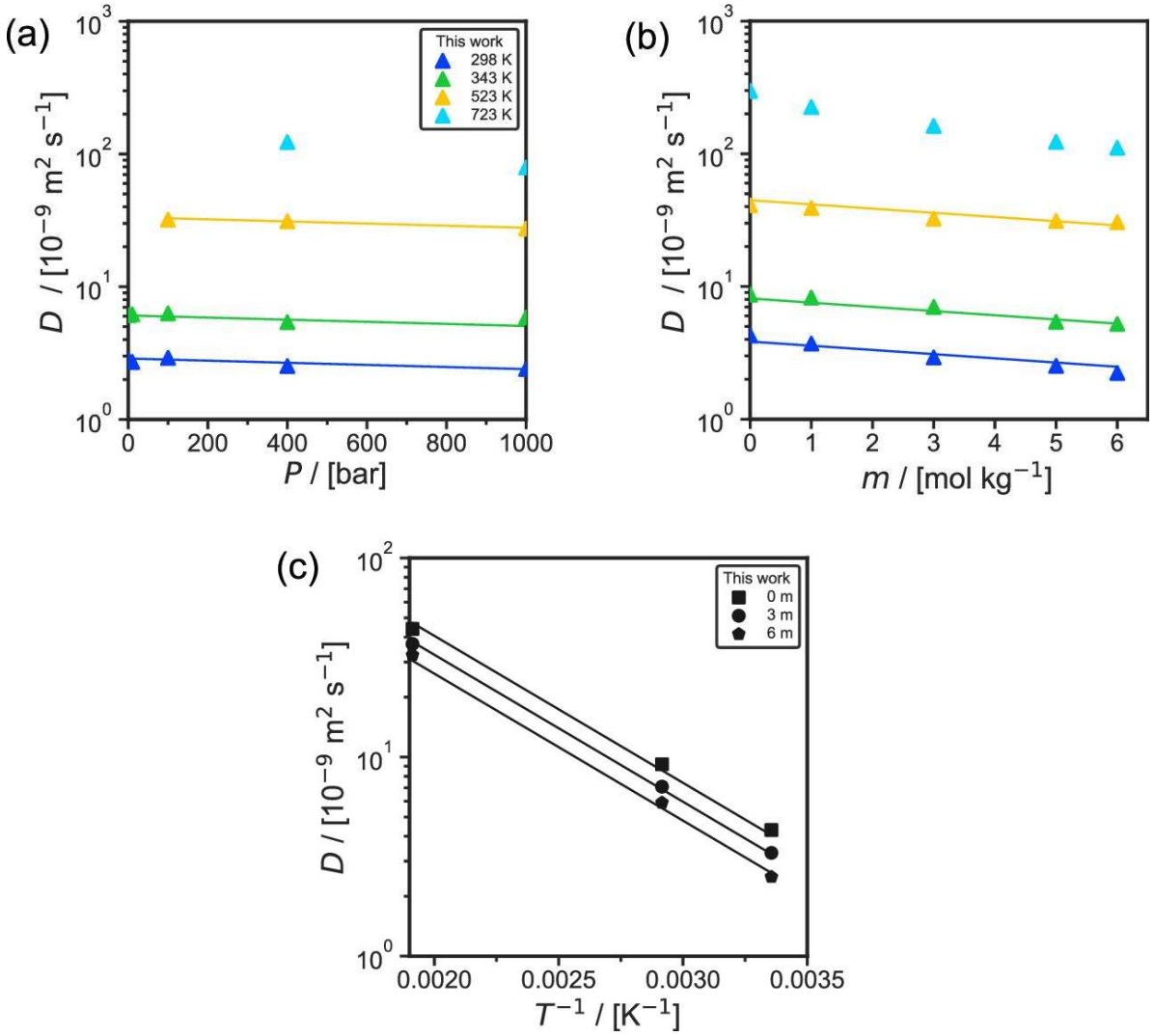

Fig. 22. Computed finite-size corrected D_{H_2} in aqueous NaCl solutions as a function of (a) pressure at constant molality of 5 mol NaCl/kg H_2O solution for varying temperatures of 298 to 723 K, (b) molality of the solution at a constant pressure of 400 bar for varying temperatures of 298 to 723 K, and (c) reciprocal temperature at 100 bar constant pressure for varying molalities of 0 to 6 NaCl/kg H_2O solution. Note that the solid lines represent the calculated fitted values [39].

Conversely, in the case of molality as shown in **Figure 22(b)**, the logarithm of hydrogen self-diffusivities was found to decrease linearly with increasing NaCl molality. This behaviour is attributed to the exponential increase in viscosity of aqueous NaCl solutions with increasing NaCl molality, as reported by Laliberté, [133]. Specifically, Laliberté observed that the viscosities of aqueous NaCl solutions increase exponentially with increasing NaCl molality, and since the diffusivities of gases in liquids are inversely proportional to the solution

viscosities, this, therefore, accounts for the observed linear trend [133]. Finally, the influence of temperature was examined by van Rooijen et al. [39] as shown in the panel of **Figure 22(c)**. They observed that the self-diffusivity of hydrogen follows an Arrhenius-type relation $\left(D \propto exp\left[\frac{c}{T}\right]\right)$, which is consistent with the behavior of gases such as O_2 and CO_2 when dissolved in aqueous solvents [132,134].

7. Perspective

Existing studies in literature have shown that high IFT exists in reservoir at the H_2-brine interface due to solubility and density contrast. High IFT is desirable for H_2 storage in underground reservoirs because it ensures the different gas phases do not mix. Moreover, at high IFT, H_2 can be safely stored in the reservoir with lowered risk of geo-mechanical failure [23]. On the other hand, a low IFT of H_2 and other gases is favourable during withdrawal schemes of H_2 from reservoirs to enable gas stored in pores of the reservoir rock system to easily flow to the surface during production. Future research should consider determining the optimal IFT suitable for the storage and production of H_2 in porous geologic formations.

Furthermore, wettability alteration studies on host rock, caprock, and representative reservoir rock systems have demonstrated strongly water-wetting condition in the presence of H_2-brine [103,135]. This indicates that the H_2 does not wet the surface of the reservoir rock system and portends good storage efficiency for H_2 in geological porous media. Moreover, since H_2 cannot displace the water layer on the caprock, the sealing efficiency of the rock is protected, thereby preventing potential losses due to leakage, and ensuring containment security. However, *in situ* studies of H_2-brine wettability in porous media have shown that water-wetting condition of reservoir rock system also increases the residual and capillary trapping potential of H_2 in the formation [102,136]. Increasing residual and capillary trapping of H_2 in geologic formation is undesired due to its negative effect on withdrawal efficiency of H_2 from reservoir formation. The residual and capillary trapping effect of H_2 in the water-wet formation can be minimized via the introduction of cushion gas such as CH_4, N_2, and CO_2 [137,138]. Nonetheless, the introduction of cushion gas instigates the issue of unavoidable gas mixing. The gas mixing process contaminates the H_2 purity during withdrawal process. To this end, some authors have opined the use of H_2 as a cushion gas during the storage process. Nevertheless, this will increase the project economics as this implies that more H_2 will be required for the cushioning process. In our view, the issue of unavoidable gas mixing that may be encountered due to the

introduction of cushion gas can be solved via the installation of an efficient and effective H_2-permeable membrane in the producer well during the withdrawal process. The H_2-membrane will selectively allow the passage of H_2 while retaining other associated gases in the geologic formation.

Adsorption of hydrogen on pure reservoir rock system is low compared to other gases such as N_2, CO_2, and CH_4. This is due to the low density of H_2 gas on the rock surface. Contrarily, rock surface contaminated with organic acid tends to have a higher wettability and become H_2-wet. This can be adduced to the adsorption of the molecules of organic acid on the surface of the rock, thereby increasing its hydrophobicity. The increased hydrophobicity introduced by the organic acid causes de-wetting of water molecules, and resultantly increased spreading of H_2 on the rock surface. Low adsorption of H_2 gas recorded on rock surface is desirable for good storage efficiency and subsequent withdrawal from the geologic formations.

Additionally, the effect of inherent reservoir parameters such as temperature, pressure, salinity, and organic acid concentration on reservoir rock-fluid and fluid-fluid properties during UHS have been studied. The outcome of numerous studies of inherent reservoir parameters on storage efficiency of H_2 have showed some discrepancies in literature. For example, some studies showed no significant effect of temperature and pressure on the IFT and wettability of reservoir rock system while other studies noted slight to notable changes. Based on the reported studies, we observed that the changes in method for conducting the experiment may have caused the changes observed in some experiment. For example, Al-Mukainah et al. [58] presented a new method to conduct sessile drop method by using the same drop of water to conduct contact angle measurements at varying pressure by gradually pressurizing with H_2. The method reported is different from that adopted in other studies whereby different brine droplet is used. Also, while some studies preferred sessile drop method, other studies were conducted using captive bubble, and core flooding incorporated with *in situ* X-ray tomography. To overcome the discrepancies reported for inherent reservoir parameters on storage efficiency, a standard approach devoid of uncertainties needs to be developed. Furthermore, it is noteworthy that the inherent reservoir parameters have implications for withdrawal efficiency of H_2 from geologic formations. For example, low pressure sites were recommended for future hydrogen storage projects because increasing pressure (characteristic of deeper reservoirs) was found to increase residually trapped H_2, thereby reducing recovery during imbibition process [136]. Similarly, increasing organic acid concentration causes increased wetting, adsorption,

and retention of H_2 in geologic porous media. Meanwhile, H_2 recovery increased with injection of brine at high capillary number. Undoubtedly, the optimization of inherent reservoir parameters is required to achieve the desired H_2 storage and withdrawal efficiency.

8. Conclusion and recommendation

UHS has been identified as a promising option for storing hydrogen and reducing greenhouse gas emissions. Various geological formations have been studied as potential storage sites, and advancements in technology and modelling have made it possible to accurately predict the performance and safety of these storage facilities. An adequate understanding of fluid-fluid and fluid-rock interactions is of fundamental importance as it plays a dominant role in the distribution of the injected fluid within the reservoir's pore space. More importantly, it dictates the maximum amount of fluid that can be withdrawn from the reservoir from these storage media. Herein, we have expounded on these influencing parameters with emphasis on solubility, interfacial tension (fluid-fluid and rock-fluid), wettability, adsorption, and diffusivity to comprehend the underpinning interactions between the injected H_2 gas, reservoir fluids, and geologic rock surface. Based on the extensive analysis of fluid-fluid and fluid-rock interactions in UHS, there are certain knowledge gaps that need to be addressed for the successful implementation of future UHS projects. These gaps are outlined as follows:

- Optimization of critical factors that govern the hydrodynamics of UHS processes is required to improve process efficiency.
- A systematic approach that allows for the quantification of adsorption and desorption of H_2 gas on a typical reservoir rock system is desired. Moreover, the influence of temperature, pressure, salinity, and reservoir surface area typical of the geologic porous medium on the long-term adsorption and desorption process should be evaluated.
- Large datasets in the literature concerning the effect of salinity on UHS processes have focussed on investigating the use of sodium chloride (NaCl) solution as a representative of formation brine. Under real reservoir conditions, formation brine is a mixture of monovalent, divalent, and sometimes trivalent ions. Further research that considers the admixture of brine should be considered in future studies as they are more representative of typical reservoir conditions.
- Due to its low molecular weight and viscosity, the H_2 diffusion process causes a viscous fingering phenomenon which may result in H_2 loss during UHS. Thus far, extensive diffusivity studies of hydrogen into nanopores and micropores of depleted oil/gas

reservoir is lacking in the literature. Multiscale adsorption and diffusion modelling studies capable of estimating H_2 loss during UHS in depleted oil/gas reservoirs are recommended for further studies.

- Finally, considerable further research is required to fully understand the interplay of interactions at the pore scale during UHS.

Nomenclature

CA	Contact angle
$CaCl_2$	Calcium Chloride
CH_4	Methane
CO_2	Carbon dioxide
DFT	Density Functional Theory
GHG	Green House Gas
HA	Humic Acid
H_2	Hydrogen
H_2O	Water
IFT	Interfacial tension
KCl	Potassium Chloride
KI	Potassium Iodide
$MgCl_2$	Magnesium Chloride
$MgSO_4$	Magnesium sulfate
NaCl	Sodium Chloride
Na_2SO_4	Sodium sulfate
N_2	Nitrogen
NO_2	Nitrous oxide
OA	Organic acids

TOC	Total Organic Content
UGS	Underground Gas Storage
UHS	Underground Hydrogen Storage
$\mu - CT$	Micro Computerized Tomography
ρ	Density (kg/m^3)
$\Delta\rho$	Liquid and gas density difference (kg/m^3)
θ	Contact angle (^{o})
θ_a	Advancing CA (^{o})
θ_r	Receding CA (^{o})
γ	IFT (mN/m)
$\gamma_{fluid-brine}$	Fluid brine IFT (mN/m)
$\gamma_{fluid-gas}$	Fluid gas IFT (mN/m)
$\gamma_{rock-brine}$	Rock brine IFT (mN/m)
$\gamma_{rock-gas}$	Rock gas IFT (mN/m)
D_{H_2}	Hydrogen diffusivity (m^2/s)

Acknowledgment

The authors wish to appreciate the College of Petroleum and Geosciences, King Fahd University of Petroleum and Minerals for supporting this research via the provision of unrestricted access to academic databases and resources used for writing this work.

Authors contribution

Afeez O. Gbadamosi: Conceptualization, Investigation, Data curation, Writing – original draft. **Nasiru S. Muhammed:** Conceptualization, Methodology, Investigation, Data curation, Writing – original draft. **Shirish Patil:** Project administration, Formal analysis, Supervision. **Dhafer Al Shehri:** Resources, Formal analysis, Supervision. **Muhammad Shahzad Kamal:** Writing – review & editing. **Bashirul Haq:** Writing – review & editing, **Emmanuel I. Epelle:** Writing – review & editing. **Mohammed Mahmoud:** Supervision, Formal analysis, Editing.

Conflict of Interest

The authors declare that they have no known competing financial interests or personal relationships that could have appeared to influence the work reported in this paper.

References

[1] A.M. Abdalla, S. Hossain, O.B. Nisfindy, A.T. Azad, M. Dawood, A.K. Azad, Hydrogen production, storage, transportation and key challenges with applications: A review, Energy Convers. Manag. 165 (2018) 602–627. https://doi.org/10.1016/j.enconman.2018.03.088.

[2] E.I. Epelle, K.S. Desongu, W. Obande, A.A. Adeleke, P.P. Ikubanni, J.A. Okolie, B. Gunes, A comprehensive review of hydrogen production and storage: A focus on the role of nanomaterials, Int. J. Hydrogen Energy. 47 (2022) 20398–20431. https://doi.org/10.1016/j.ijhydene.2022.04.227.

[3] B. Haq, N. Salahu Muhammed, J. Liu, H. Tong Chua, Enhanced natural gas production using CO2 injection: Application to sustainable hydrogen production, Fuel. 347 (2023) 128474. https://doi.org/10.1016/j.fuel.2023.128474.

[4] A. Gbadamosi, S. Patil, D. Al Shehri, M.S. Kamal, S.M.S. Hussain, E.W. Al-Shalabi, A.M. Hassan, Recent advances on the application of low salinity waterflooding and chemical enhanced oil recovery, Energy Reports. 8 (2022) 9969–9996. https://doi.org/10.1016/j.egyr.2022.08.001.

[5] S.E. Hosseini, M.A. Wahid, Hydrogen production from renewable and sustainable energy resources: Promising green energy carrier for clean development, Renew. Sustain. Energy Rev. 57 (2016) 850–866. https://doi.org/10.1016/j.rser.2015.12.112.

[6] S. Sharma, S.K. Ghoshal, Hydrogen the future transportation fuel: From production to applications, Renew. Sustain. Energy Rev. 43 (2015) 1151–1158. https://doi.org/https://doi.org/10.1016/j.rser.2014.11.093.

[7] C.J. Okere, J.J. Sheng, Review on clean hydrogen generation from petroleum reservoirs: Fundamentals, mechanisms, and field applications, Int. J. Hydrogen Energy. (2023) in press. https://doi.org/https://doi.org/10.1016/j.ijhydene.2023.06.135.

[8] D. Sui, E. Wiktorski, M. Røksland, T.A. Basmoen, Review and investigations on geothermal energy extraction from abandoned petroleum wells, J. Pet. Explor. Prod. Technol. 9 (2019) 1135–1147. https://doi.org/10.1007/s13202-018-0535-3.

[9] S.L. Gbadamosi, N.I. Nwulu, Y. Sun, Multi-objective optimisation for composite generation and transmission expansion planning considering offshore wind power and feed-in tariffs, IET Renew. Power Gener. 12 (2018) 1687–1697. https://doi.org/https://doi.org/10.1049/iet-rpg.2018.5531.

[10] A. Raza, M. Arif, G. Glatz, M. Mahmoud, M. Al Kobaisi, S. Alafnan, S. Iglauer, A holistic overview of underground hydrogen storage: Influencing factors, current understanding, and outlook, Fuel. 330 (2022) 125636. https://doi.org/10.1016/j.fuel.2022.125636.

[11] R. Tarkowski, B. Uliasz-Misiak, Towards underground hydrogen storage: A review of barriers, Renew. Sustain. Energy Rev. 162 (2022) 112451. https://doi.org/10.1016/j.rser.2022.112451.

[12] K. Anaya, A. Olufemi Oni, A. Kumar, Investigating the techno-economic and environmental performance of chemical looping technology for hydrogen production, Sustain. Energy Technol. Assessments. 56 (2023) 103008. https://doi.org/https://doi.org/10.1016/j.seta.2022.103008.

[13] J. Tang, M. Chu, F. Li, C. Feng, Z. Liu, Y. Zhou, Development and progress on hydrogen metallurgy, Int. J. Miner. Metall. Mater. 27 (2020) 713–723. https://doi.org/10.1007/s12613-020-2021-4.

[14] T. Yusaf, A.S. Faisal Mahamude, K. Kadirgama, D. Ramasamy, K. Farhana, H. Al Dhahad, A.B.D.R. Abu Talib, Sustainable hydrogen energy in aviation – A narrative review, Int. J. Hydrogen Energy. (2023) in press. https://doi.org/https://doi.org/10.1016/j.ijhydene.2023.02.086.

[15] L. Fan, Z. Tu, S.H. Chan, Recent development of hydrogen and fuel cell technologies: A review, Energy Reports. 7 (2021) 8421–8446. https://doi.org/10.1016/j.egyr.2021.08.003.

[16] M. Amin, H.H. Shah, A.G. Fareed, W.U. Khan, E. Chung, A. Zia, Z.U. Rahman Farooqi, C. Lee, Hydrogen production through renewable and non-renewable energy processes and their impact on climate change, Int. J. Hydrogen Energy. 47 (2022) 33112–33134. https://doi.org/10.1016/j.ijhydene.2022.07.172.

[17] V. Mirchi, M. Dejam, V. Alvarado, Interfacial tension and contact angle measurements for hydrogen-methane mixtures/brine/oil-wet rocks at reservoir conditions, Int. J. Hydrogen Energy. 47 (2022) 34963–34975. https://doi.org/10.1016/j.ijhydene.2022.08.056.

[18] A. Hassanpouryouzband, E. Joonaki, K. Edlmann, N. Heinemann, J. Yang, Thermodynamic and transport properties of hydrogen containing streams, Sci. Data. 7 (2020) 1–14. https://doi.org/10.1038/s41597-020-0568-6.

[19] A. Hassanpouryouzband, K. Adie, T. Cowen, E.M. Thaysen, N. Heinemann, I.B. Butler, M. Wilkinson, K. Edlmann, Geological Hydrogen Storage: Geochemical Reactivity of Hydrogen with Sandstone Reservoirs, ACS Energy Lett. 7 (2022) 2203–2210. https://doi.org/10.1021/acsenergylett.2c01024.

[20] C. Sambo, A. Dudun, S.A. Samuel, P. Esenenjor, N.S. Muhammed, B. Haq, A review on worldwide underground hydrogen storage operating and potential fields, Int. J. Hydrogen Energy. 47 (2022) 22840–22880. https://doi.org/10.1016/j.ijhydene.2022.05.126.

[21] T. Amirthan, M.S.A. Perera, The role of storage systems in hydrogen economy: A review, J. Nat. Gas Sci. Eng. 108 (2022) 104843. https://doi.org/10.1016/j.jngse.2022.104843.

[22] P. Kumar, S. Singh, S.A.R. Hashmi, K.-H. Kim, MXenes: Emerging 2D materials for hydrogen storage, Nano Energy. 85 (2021) 105989. https://doi.org/https://doi.org/10.1016/j.nanoen.2021.105989.

[23] A. Hassanpouryouzband, E. Joonaki, K. Edlmann, R.S. Haszeldine, Offshore Geological Storage of Hydrogen: Is This Our Best Option to Achieve Net-Zero?, ACS Energy Lett. (2021) 2181–2186. https://doi.org/10.1021/acsenergylett.1c00845.

[24] A.W.C. van den Berg, C.O. Areán, Materials for hydrogen storage: current research trends and perspectives, Chem. Commun. (2008) 668–681. https://doi.org/10.1039/B712576N.

[25] J. Ren, N.M. Musyoka, H.W. Langmi, M. Mathe, S. Liao, Current research trends and perspectives on materials-based hydrogen storage solutions: A critical review, Int. J. Hydrogen Energy. 42 (2017) 289–311. https://doi.org/10.1016/j.ijhydene.2016.11.195.

[26] H. Hematpur, R. Abdollahi, S. Rostami, M. Haghighi, M.J. Blunt, Advances in Review

of underground hydrogen storage : Concepts and challenges, 7 (2023) 111–131. https://doi.org/doi.org/10.46690/ager.2023.02.05.

[27] H. Bin Navaid, H. Emadi, M. Watson, A comprehensive literature review on the challenges associated with underground hydrogen storage, Int. J. Hydrogen Energy. 48 (2023) 10603–10635. https://doi.org/10.1016/j.ijhydene.2022.11.225.

[28] A. Aftab, A. Hassanpouryouzband, H. Naderi, Q. Xie, M. Sarmadivaleh, Quantifying onshore salt deposits and their potential for hydrogen energy storage in Australia, J. Energy Storage. 65 (2023) 107252. https://doi.org/https://doi.org/10.1016/j.est.2023.107252.

[29] T. Amirthan, M.S.A. Perera, Underground hydrogen storage in Australia: A review on the feasibility of geological sites, Int. J. Hydrogen Energy. (2022). https://doi.org/10.1016/j.ijhydene.2022.10.218.

[30] N.S. Muhammed, M.B. Haq, D.A. Al Shehri, A. Al-Ahmed, M.M. Rahman, E. Zaman, S. Iglauer, Hydrogen storage in depleted gas reservoirs: A comprehensive review, Fuel. 337 (2023) 127032. https://doi.org/10.1016/j.fuel.2022.127032.

[31] N.S. Muhammed, B. Haq, D. Al Shehri, A. Al-Ahmed, M.M. Rahman, E. Zaman, A review on underground hydrogen storage: Insight into geological sites, influencing factors and future outlook, Energy Reports. 8 (2022) 461–499. https://doi.org/10.1016/j.egyr.2021.12.002.

[32] M.S.A. Perera, A review of underground hydrogen storage in depleted gas reservoirs: Insights into various rock-fluid interaction mechanisms and their impact on the process integrity, Fuel. 334 (2023) 126677. https://doi.org/10.1016/j.fuel.2022.126677.

[33] N. Heinemann, J. Alcalde, J.M. Miocic, S.J.T. Hangx, J. Kallmeyer, C. Ostertag-Henning, A. Hassanpouryouzband, E.M. Thaysen, G.J. Strobel, C. Schmidt-Hattenberger, K. Edlmann, M. Wilkinson, M. Bentham, R. Stuart Haszeldine, R. Carbonell, A. Rudloff, Enabling large-scale hydrogen storage in porous media – the scientific challenges, Energy Environ. Sci. 14 (2021) 853–864. https://doi.org/10.1039/D0EE03536J.

[34] D. Zivar, S. Kumar, J. Foroozesh, Underground hydrogen storage: A comprehensive review, Int. J. Hydrogen Energy. 46 (2021) 23436–23462. https://doi.org/10.1016/j.ijhydene.2020.08.138.

[35] A. Aftab, A. Hassanpouryouzband, Q. Xie, L.L. Machuca, M. Sarmadivaleh, Toward a Fundamental Understanding of Geological Hydrogen Storage, Ind. Eng. Chem. Res. 61 (2022) 3233–3253. https://doi.org/10.1021/acs.iecr.1c04380.

[36] E.I. Epelle, W. Obande, G.A. Udourioh, I.C. Afolabi, K.S. Desongu, U. Orivri, B. Gunes, J.A. Okolie, Perspectives and prospects of underground hydrogen storage and natural hydrogen, Sustain. Energy Fuels. 6 (2022) 3324–3343. https://doi.org/10.1039/D2SE00618A.

[37] M. Aslannezhad, M. Ali, A. Kalantariasl, M. Sayyafzadeh, Z. You, S. Iglauer, A. Keshavarz, A review of hydrogen/rock/brine interaction: Implications for Hydrogen Geo-storage, Prog. Energy Combust. Sci. 95 (2023) 101066. https://doi.org/10.1016/j.pecs.2022.101066.

[38] Z. Pan, J.P.M. Trusler, Experimental and modelling study of the interfacial tension of (n-decane + carbon dioxide + water) in the three phase region, Fluid Phase Equilib. 568 (2023) 113760. https://doi.org/10.1016/j.fluid.2023.113760.

[39] W.A. van Rooijen, P. Habibi, K. Xu, P. Dey, T.J.H. Vlugt, H. Hajibeygi, O.A. Moultos, Interfacial Tensions, Solubilities, and Transport Properties of the H 2 /H 2 O/NaCl System: A Molecular Simulation Study, J. Chem. Eng. Data. (2023). https://doi.org/10.1021/acs.jced.2c00707.

[40] J. Alvarez, R. Crovetto, R. Fernandez-Prini, Dissolution of N2 and of H2 in Water From Room Temperature To 640 K., Berichte Der Bunsengesellschaft/Physical Chem. Chem. Phys. 92 (1988) 935–940. https://doi.org/10.1002/bbpc.198800223.

[41] S. Chabab, P. Théveneau, C. Coquelet, J. Corvisier, P. Paricaud, Measurements and predictive models of high-pressure H2 solubility in brine (H2O+NaCl) for underground hydrogen storage application, Int. J. Hydrogen Energy. 45 (2020) 32206–32220. https://doi.org/10.1016/j.ijhydene.2020.08.192.

[42] S. P, Ueber die Absorption des Wasserstoffs im Wasser und in wasserigen¨ Lösungen, Ann. Phys. (1893) 275–299.

[43] T.E. Crozier, S. Yamamoto, Solubility of Hydrogen in Water , Seawater , and NaCI Solutions, J. Chem. Eng. Data. 19 (1974) 242–244.

[44] P. Press, G. Britain, R. Standley, The solubility of molecular hydrogen in seawater, Deep. Res. 24 (1977) 937–941.

[45] R. Wiebe, V.L. Gaddy, B.R. Wiebe, The Solubility of Hydrogen in Water at 0, 50, 75 and 100° from 25 to 1000 Atmospheres Atmospheres, J. Am. Chem. Soc. 50 (1934).

[46] L. Braun, Über die Absorption von Stickstoff und von Wasserstoff in wässerigen Lösungen verschieden dissociierter Stoffe ., Phys. Chem. 8 (1897) 721–739.

[47] G.A. Torín-Ollarves, J.P.M. Trusler, Solubility of hydrogen in sodium chloride brine at high pressures, Fluid Phase Equilib. 539 (2021) 113025. https://doi.org/10.1016/j.fluid.2021.113025.

[48] S. Ansari, M. Safaei-Farouji, S. Atashrouz, A. Abedi, A. Hemmati-Sarapardeh, A. Mohaddespour, Prediction of hydrogen solubility in aqueous solutions: Comparison of equations of state and advanced machine learning-metaheuristic approaches, Int. J. Hydrogen Energy. 47 (2022) 37724–37741. https://doi.org/10.1016/j.ijhydene.2022.08.288.

[49] D. Li, C. Beyer, S. Bauer, A unified phase equilibrium model for hydrogen solubility and solution density, Int. J. Hydrogen Energy. 43 (2018) 512–529. https://doi.org/10.1016/j.ijhydene.2017.07.228.

[50] C. Lopez-Lazaro, P. Bachaud, I. Moretti, N. Ferrando, Predicting the phase behavior of hydrogen in NaCl brines by molecular simulation for geological applications, BSGF - Earth Sci. Bull. 190 (2019). https://doi.org/10.1051/bsgf/2019008.

[51] R. Gholami, Hydrogen storage in geological porous media: Solubility, mineral trapping, H2S generation and salt precipitation, J. Energy Storage. 59 (2023) 106576. https://doi.org/https://doi.org/10.1016/j.est.2022.106576.

[52] B. Pan, X. Yin, Y. Ju, S. Iglauer, Underground hydrogen storage: Influencing parameters and future outlook, Adv. Colloid Interface Sci. 294 (2021) 102473. https://doi.org/10.1016/j.cis.2021.102473.

[53] M.A. Gallardo, M.C. López, J.S. Urieta, C.G. Losa, Solubility of 15 non-polar gases (He, Ne, Ar, Kr, Xe, H2, D2, N2, O2, CH4, C2H4, C2H6, CF4, SF6 and CO2) in cycloheptanone, Fluid Phase Equilib. 58 (1990) 159–172. https://doi.org/10.1016/0378-3812(90)87011-D.

[54] K.M. Joshi, S.C. Saxena, Viscosity of polar gases, Physica. 27 (1961) 329–336. https://doi.org/10.1016/0031-8914(61)90105-7.

[55] S. Raeissi, C.J. Peters, Understanding temperature dependency of hydrogen solubility in

ionic liquids, including experimental data in [bmim][Tf 2 N], AIChE J. 58 (2012) 3553–3559. https://doi.org/10.1002/aic.13742.

[56] S. Higgs, Y. Da Wang, C. Sun, J. Ennis-King, S.J. Jackson, R.T. Armstrong, P. Mostaghimi, In-situ hydrogen wettability characterisation for underground hydrogen storage, Int. J. Hydrogen Energy. 47 (2022) 13062–13075. https://doi.org/10.1016/j.ijhydene.2022.02.022.

[57] Y.T.F. Chow, G.C. Maitland, J.P.M. Trusler, Interfacial tensions of (H2O + H2) and (H2O + CO2 + H2) systems at temperatures of (298–448) K and pressures up to 45 MPa, Fluid Phase Equilib. 475 (2018) 37–44. https://doi.org/10.1016/j.fluid.2018.07.022.

[58] H. Al-Mukainah, A. Al-Yaseri, N. Yekeen, J. Al Hamad, M. Mahmoud, Wettability of shale–brine–H2 system and H2-brine interfacial tension for assessment of the sealing capacities of shale formations during underground hydrogen storage, Energy Reports. 8 (2022) 8830–8843. https://doi.org/10.1016/j.egyr.2022.07.004.

[59] M. Hosseini, J. Fahimpour, M. Ali, A. Keshavarz, S. Iglauer, H2−brine interfacial tension as a function of salinity, temperature, and pressure; implications for hydrogen geo-storage, J. Pet. Sci. Eng. 213 (2022) 110441. https://doi.org/10.1016/j.petrol.2022.110441.

[60] H. Esfandyari, M. Sarmadivaleh, F. Esmaeilzadeh, M. Ali, S. Iglauer, A. Keshavarz, Experimental evaluation of rock mineralogy on hydrogen-wettability: Implications for hydrogen geo-storage, J. Energy Storage. 52 (2022) 104866. https://doi.org/10.1016/j.est.2022.104866.

[61] B.E. Poling, J.M. Prausnitz, J.P. O'Connell, The Properties of Gases and Liquids, 2001.

[62] Z. Dalal Isfehani, A. Sheidaie, M. Hosseini, J. Fahimpour, S. Iglauer, A. Keshavarz, Interfacial tensions of (brine + H2 + CO2) systems at gas geo-storage conditions, J. Mol. Liq. 374 (2023) 121279. https://doi.org/10.1016/j.molliq.2023.121279.

[63] Y. Levin, A.P. dos Santos, A. Diehl, Ions at the Air-Water Interface: An End to a Hundred-Year-Old Mystery?, Phys. Rev. Lett. 103 (2009) 257802. https://doi.org/10.1103/PhysRevLett.103.257802.

[64] C.A. Aggelopoulos, M. Robin, O. Vizika, Interfacial tension between CO2 and brine (NaCl+CaCl2) at elevated pressures and temperatures: The additive effect of different salts, Adv. Water Resour. 34 (2011) 505–511.

https://doi.org/10.1016/j.advwatres.2011.01.007.

[65] M. Manciu, E. Ruckenstein, Specific ion effects via ion hydration: I. Surface tension, Adv. Colloid Interface Sci. 105 (2003) 63–101. https://doi.org/10.1016/S0001-8686(03)00018-6.

[66] Y. Marcus, Effect of ions on the structure of water, Pure Appl. Chem. 82 (2010) 1889–1899. https://doi.org/10.1351/PAC-CON-09-07-02.

[67] L.M. Pegram, M.T. Record, Hofmeister salt effects on surface tension arise from partitioning of anions and cations between bulk water and the air-water interface, J. Phys. Chem. B. 111 (2007) 5411–5417. https://doi.org/10.1021/jp070245z.

[68] S. Weisenberger, A. Schumpe, Estimation of gas solubilities in salt solutions at temperatures from 273 K to 363 K, AIChE J. 42 (1996) 298–300. https://doi.org/10.1002/aic.690420130.

[69] N. Heinemann, J. Scafidi, G. Pickup, E.M. Thaysen, A. Hassanpouryouzband, M. Wilkinson, A.K. Satterley, M.G. Booth, K. Edlmann, R.S. Haszeldine, Hydrogen storage in saline aquifers: The role of cushion gas for injection and production, Int. J. Hydrogen Energy. 46 (2021) 39284–39296. https://doi.org/10.1016/j.ijhydene.2021.09.174.

[70] M. Zamehrian, B. Sedaee, Underground hydrogen storage in a partially depleted gas condensate reservoir: Influence of cushion gas, J. Pet. Sci. Eng. 212 (2022) 110304. https://doi.org/10.1016/j.petrol.2022.110304.

[71] A. Alanazi, N. Yekeen, M. Ali, M. Ali, I.S. Abu-Mahfouz, A. Keshavarz, S. Iglauer, H. Hoteit, Influence of organics and gas mixing on hydrogen/brine and methane/brine wettability using Jordanian oil shale rocks: Implications for hydrogen geological storage, J. Energy Storage. 62 (2023) 106865. https://doi.org/10.1016/j.est.2023.106865.

[72] A. Alanazi, N. Yekeen, M. Ali, M. Ali, I.S. Abu-Mahfouz, A. Keshavarz, S. Iglauer, H. Hoteit, Influence of organics and gas mixing on hydrogen/brine and methane/brine wettability using Jordanian oil shale rocks: Implications for hydrogen geological storage, J. Energy Storage. 62 (2023) 106865. https://doi.org/10.1016/j.est.2023.106865.

[73] H. Al-Mukainah, A. Al-Yaseri, N. Yekeen, J. Al Hamad, M. Mahmoud, Wettability of

shale–brine–H2 system and H2-brine interfacial tension for assessment of the sealing capacities of shale formations during underground hydrogen storage, Energy Reports. 8 (2022) 8830–8843. https://doi.org/10.1016/j.egyr.2022.07.004.

[74] M. Lysyy, M. Fernø, G. Ersland, Seasonal hydrogen storage in a depleted oil and gas field, Int. J. Hydrogen Energy. 46 (2021) 25160–25174. https://doi.org/10.1016/j.ijhydene.2021.05.030.

[75] Z. Shi, K. Jessen, T.T. Tsotsis, Impacts of the subsurface storage of natural gas and hydrogen mixtures, Int. J. Hydrogen Energy. 45 (2020) 8757–8773. https://doi.org/10.1016/j.ijhydene.2020.01.044.

[76] B. Pan, X. Yin, S. Iglauer, Rock-fluid interfacial tension at subsurface conditions: Implications for H2, CO2 and natural gas geo-storage, Int. J. Hydrogen Energy. 46 (2021) 25578–25585. https://doi.org/10.1016/j.ijhydene.2021.05.067.

[77] M. Ali, B. Pan, N. Yekeen, S. Al-Anssari, A. Al-Anazi, A. Keshavarz, S. Iglauer, H. Hoteit, Assessment of wettability and rock-fluid interfacial tension of caprock: Implications for hydrogen and carbon dioxide geo-storage, Int. J. Hydrogen Energy. 47 (2022) 14104–14120. https://doi.org/10.1016/j.ijhydene.2022.02.149.

[78] N. Yekeen, A. Al-Yaseri, B.M. Negash, M. Ali, A. Giwelli, L. Esteban, J. Sarout, Clay-hydrogen and clay-cushion gas interfacial tensions: Implications for hydrogen storage, Int. J. Hydrogen Energy. 47 (2022) 19155–19167. https://doi.org/10.1016/j.ijhydene.2022.04.103.

[79] H. Esfandyari, M. Hosseini, M. Ali, S. Iglauer, M. Haghighi, A. Keshavarz, Assessment of the interfacial properties of various mineral/hydrogen/water systems, J. Energy Storage. 60 (2023) 106637. https://doi.org/10.1016/j.est.2023.106637.

[80] M. Hosseini, M. Ali, J. Fahimpour, A. Keshavarz, S. Iglauer, Calcite–Fluid Interfacial Tension: H2 and CO2 Geological Storage in Carbonates, Energy & Fuels. 37 (2023) 5986–5994. https://doi.org/10.1021/acs.energyfuels.3c00399.

[81] M. Hosseini, M. Ali, J. Fahimpour, A. Keshavarz, S. Iglauer, Assessment of rock-hydrogen and rock-water interfacial tension in shale, evaporite and basaltic rocks, J. Nat. Gas Sci. Eng. 106 (2022) 104743. https://doi.org/10.1016/j.jngse.2022.104743.

[82] L. Hashemi, W. Glerum, R. Farajzadeh, H. Hajibeygi, Contact angle measurement for hydrogen/brine/sandstone system using captive-bubble method relevant for

underground hydrogen storage, Adv. Water Resour. 154 (2021) 103964. https://doi.org/10.1016/j.advwatres.2021.103964.

[83] L. Zeng, M. Hosseini, A. Keshavarz, S. Iglauer, Y. Lu, Q. Xie, Hydrogen wettability in carbonate reservoirs: Implication for underground hydrogen storage from geochemical perspective, Int. J. Hydrogen Energy. 47 (2022) 25357–25366. https://doi.org/10.1016/j.ijhydene.2022.05.289.

[84] M. Hosseini, J. Fahimpour, M. Ali, A. Keshavarz, S. Iglauer, Hydrogen wettability of carbonate formations: Implications for hydrogen geo-storage, J. Colloid Interface Sci. 614 (2022) 256–266. https://doi.org/10.1016/j.jcis.2022.01.068.

[85] J. Hou, S. Lin, M. Zhang, W. Li, Salinity, temperature and pressure effect on hydrogen wettability of carbonate rocks, Int. J. Hydrogen Energy. (2022). https://doi.org/10.1016/j.ijhydene.2022.05.274.

[86] M. Ali, N.K. Jha, A. Al-Yaseri, Y. Zhang, S. Iglauer, M. Sarmadivaleh, Hydrogen wettability of quartz substrates exposed to organic acids; Implications for hydrogen geo-storage in sandstone reservoirs, J. Pet. Sci. Eng. 207 (2021) 109081. https://doi.org/10.1016/j.petrol.2021.109081.

[87] S. Iglauer, M. Ali, A. Keshavarz, Hydrogen Wettability of Sandstone Reservoirs: Implications for Hydrogen Geo-Storage, Geophys. Res. Lett. 48 (2021) 1–5. https://doi.org/10.1029/2020GL090814.

[88] M. Ali, N. Yekeen, N. Pal, A. Keshavarz, S. Iglauer, H. Hoteit, Influence of organic molecules on wetting characteristics of mica/H2/brine systems: Implications for hydrogen structural trapping capacities, J. Colloid Interface Sci. 608 (2022) 1739–1749. https://doi.org/10.1016/j.jcis.2021.10.080.

[89] A. Al-Yaseri, N. Yekeen, M. Mahmoud, A. Kakati, Q. Xie, A. Giwelli, Thermodynamic characterization of H2-brine-shale wettability: Implications for hydrogen storage at subsurface, Int. J. Hydrogen Energy. 47 (2022) 22510–22521. https://doi.org/10.1016/j.ijhydene.2022.05.086.

[90] M. Ali, N. Yekeen, N. Pal, A. Keshavarz, S. Iglauer, H. Hoteit, Influence of pressure, temperature and organic surface concentration on hydrogen wettability of caprock; implications for hydrogen geo-storage, Energy Reports. 7 (2021) 5988–5996. https://doi.org/10.1016/j.egyr.2021.09.016.

[91] M. Hosseini, M. Ali, J. Fahimpour, A. Keshavarz, S. Iglauer, Basalt-H2-brine wettability at geo-storage conditions: Implication for hydrogen storage in basaltic formations, J. Energy Storage. 52 (2022) 104745. https://doi.org/10.1016/j.est.2022.104745.

[92] M. Hosseini, R. Sedev, M. Ali, M. Ali, J. Fahimpour, A. Keshavarz, S. Iglauer, Hydrogen-wettability alteration of Indiana limestone in the presence of organic acids and nanofluid, Int. J. Hydrogen Energy. (2023) in press. https://doi.org/https://doi.org/10.1016/j.ijhydene.2023.05.292.

[93] M. Hosseini, J. Fahimpour, M. Ali, A. Keshavarz, S. Iglauer, Capillary Sealing Efficiency Analysis of Caprocks: Implication for Hydrogen Geological Storage, Energy & Fuels. 36 (2022) 4065–4075. https://doi.org/10.1021/acs.energyfuels.2c00281.

[94] A. Al-Yaseri, D. Wolff-Boenisch, C.A. Fauziah, S. Iglauer, Hydrogen wettability of clays: Implications for underground hydrogen storage, Int. J. Hydrogen Energy. 46 (2021) 34356–34361. https://doi.org/10.1016/j.ijhydene.2021.07.226.

[95] L. Hashemi, M. Boon, W. Glerum, R. Farajzadeh, H. Hajibeygi, A comparative study for H2–CH4 mixture wettability in sandstone porous rocks relevant to underground hydrogen storage, Adv. Water Resour. 163 (2022). https://doi.org/10.1016/j.advwatres.2022.104165.

[96] A. Al-Yaseri, N.K. Jha, On hydrogen wettability of basaltic rock, J. Pet. Sci. Eng. 200 (2021) 108387. https://doi.org/10.1016/j.petrol.2021.108387.

[97] N.K. Jha, A. Al-Yaseri, M. Ghasemi, D. Al-Bayati, M. Lebedev, M. Sarmadivaleh, Pore scale investigation of hydrogen injection in sandstone via X-ray micro-tomography, Int. J. Hydrogen Energy. 46 (2021) 34822–34829. https://doi.org/10.1016/j.ijhydene.2021.08.042.

[98] W.T. Pfeiffer, C. Beyer, S. Bauer, Hydrogen storage in a heterogeneous sandstone formation: Dimensioning and induced hydraulic effects, Pet. Geosci. 23 (2017) 315–326. https://doi.org/10.1144/petgeo2016-050.

[99] W.T. Pfeiffer, S. Bauer, Subsurface Porous Media Hydrogen Storage - Scenario Development and Simulation, Energy Procedia. 76 (2015) 565–572. https://doi.org/10.1016/j.egypro.2015.07.872.

[100] F. Feldmann, B. Hagemann, L. Ganzer, M. Panfilov, Numerical simulation of

hydrodynamic and gas mixing processes in underground hydrogen storages, Environ. Earth Sci. 75 (2016) 1–15. https://doi.org/10.1007/s12665-016-5948-z.

[101] R. Sedev, H. Akhondzadeh, M. Ali, A. Keshavarz, S. Iglauer, Contact Angles of a Brine on a Bituminous Coal in Compressed Hydrogen, Geophys. Res. Lett. 49 (2022). https://doi.org/10.1029/2022GL098261.

[102] Z. Jangda, H. Menke, A. Busch, S. Geiger, T. Bultreys, H. Lewis, K. Singh, Pore-scale visualization of hydrogen storage in a sandstone at subsurface pressure and temperature conditions: Trapping, dissolution and wettability, J. Colloid Interface Sci. 629 (2023) 316–325. https://doi.org/10.1016/j.jcis.2022.09.082.

[103] H. Aghaei, A. Al-Yaseri, A. Toorajipour, B. Shahsavani, N. Yekeen, K. Edlmann, Host-rock and caprock wettability during hydrogen drainage: Implications of hydrogen subsurface storage, Fuel. 351 (2023) 129048. https://doi.org/https://doi.org/10.1016/j.fuel.2023.129048.

[104] H. Samara, T. Von Ostrowski, P. Jaeger, Geological Storage of Carbon Dioxide and Hydrogen in Jordanian Shale Formations, in: SPE-210202-MS, Pap. Present. SPE Annu. Tech. Conf. Exhib. Houston, Texas, USA, Oct. 2022, 2022: p. D021S029R002. https://doi.org/10.2118/210202-MS.

[105] A. Raza, M. Mahmoud, S. Alafnan, M. Arif, G. Glatz, H2, CO2, and CH4 Adsorption Potential of Kerogen as a Function of Pressure, Temperature, and Maturity, Int. J. Mol. Sci. 23 (2022) 12767. https://doi.org/10.3390/ijms232112767.

[106] H.R. Abid, N. Yekeen, A. Al-Yaseri, A. Keshavarz, S. Iglauer, The impact of humic acid on hydrogen adsorptive capacity of eagle ford shale: Implications for underground hydrogen storage, J. Energy Storage. 55 (2022) 105615. https://doi.org/https://doi.org/10.1016/j.est.2022.105615.

[107] O.J. Omotilewa, P. Panja, C. Vega-Ortiz, J. McLennan, Evaluation of enhanced coalbed methane recovery and carbon dioxide sequestration potential in high volatile bituminous coal, J. Nat. Gas Sci. Eng. 91 (2021) 103979. https://doi.org/https://doi.org/10.1016/j.jngse.2021.103979.

[108] M. Mukherjee, S. Misra, A review of experimental research on Enhanced Coal Bed Methane (ECBM) recovery via CO2 sequestration, Earth-Science Rev. 179 (2018) 392–410. https://doi.org/https://doi.org/10.1016/j.earscirev.2018.02.018.

[109] S. Iglauer, H. Abid, A. Al-Yaseri, A. Keshavarz, Hydrogen Adsorption on Sub-Bituminous Coal: Implications for Hydrogen Geo-Storage, Geophys. Res. Lett. 48 (2021) 2–5. https://doi.org/10.1029/2021GL092976.

[110] A. Keshavarz, H. Abid, M. Ali, S. Iglauer, Hydrogen diffusion in coal: Implications for hydrogen geo- storage, J. Colloid Interface Sci. 608 (2022) 1457–1462. https://doi.org/https://doi.org/10.1016/j.jcis.2021.10.050.

[111] M. Arif, H.R. Abid, A. Keshavarz, F. Jones, S. Iglauer, Hydrogen storage potential of coals as a function of pressure, temperature, and rank, J. Colloid Interface Sci. (2022). https://doi.org/10.1016/j.jcis.2022.03.138.

[112] G. Carchini, A. Hamza, I.A. Hussein, M. Saad, M. Mahmoud, R. Shawabkeh, S. Aparicio, Hydrogen storage in gas reservoirs: A molecular modeling and experimental investigation, Int. J. Hydrogen Energy. 48 (2023) 7419–7430. https://doi.org/https://doi.org/10.1016/j.ijhydene.2022.11.174.

[113] E. López-Chávez, A. Garcia-Quiroz, Y.A. Peña-Castañeda, J.A.I. Diaz-Gongora, F. de Landa Castillo-Alvarado, W.R. Carbellido, Modeling and simulation of the adsorption and storage of hydrogen in calcite rock oil fields, J. Mol. Model. 26 (2020). https://doi.org/10.1007/s00894-020-04494-2.

[114] D. Wolff-Boenisch, H.R. Abid, J.E. Tucek, A. Keshavarz, S. Iglauer, Importance of clay-H2 interactions for large-scale underground hydrogen storage, Int. J. Hydrogen Energy. (2023) in press. https://doi.org/https://doi.org/10.1016/j.ijhydene.2022.12.324.

[115] F. Bardelli, C. Mondelli, M. Didier, J.G. Vitillo, D.R. Cavicchia, J. Robinet, L. Leone, L. Charlet, Hydrogen uptake and diffusion in Callovo-Oxfordian clay rock for nuclear waste disposal technology, Appl. Geochemistry. 49 (2014) 168–177. https://doi.org/10.1016/j.apgeochem.2014.06.019.

[116] M. Didier, L. Leone, J.M. Greneche, E. Giffaut, L. Charlet, Adsorption of hydrogen gas and redox processes in clays, Environ. Sci. Technol. 46 (2012) 3574–3579. https://doi.org/10.1021/es204583h.

[117] J.E. Vivian, C.J. King, The mechanism of liquid- phase resistance to gas absorption in a packed column, AIChE J. 10 (1964) 221–227. https://doi.org/10.1002/aic.690100218.

[118] X. Zhao, H. Jin, Y. Chen, Z. Ge, Numerical study of H2, CH4, CO, O2 and CO2 diffusion in water near the critical point with molecular dynamics simulation, Comput.

Math. with Appl. 81 (2021) 759–771. https://doi.org/10.1016/j.camwa.2019.11.012.

[119] X. Zhao, H. Jin, Investigation of hydrogen diffusion in supercritical water: A molecular dynamics simulation study, Int. J. Heat Mass Transf. 133 (2019) 718–728. https://doi.org/10.1016/j.ijheatmasstransfer.2018.12.164.

[120] R.B. Bird, Transport phenomena, Appl. Mech. Rev. 55 (2002) R1–R4. https://doi.org/10.1115/1.1424298.

[121] P.O. Carden, L. Paterson, Physical, chemical and energy aspects of underground hydrogen storage, Int. J. Hydrogen Energy. 4 (1979) 559–569. https://doi.org/10.1016/0360-3199(79)90083-1.

[122] A. Akgerman, J.L. Gainer, Predicting gas-liquid diffusivities, J. Chem. Eng. Data. 17 (1972) 372–377. https://doi.org/10.1021/je60054a008.

[123] D.M. Himmelblau, Diffusion of Dissolved Gases in Liquids, Chem. Rev. 64 (1964) 527–550. https://doi.org/10.1021/cr60231a002.

[124] B. Jähne, G. Heinz, W. Dietrich, Measurement of the diffusion coefficients of sparingly soluble gases in water, J. Geophys. Res. Ocean. 92 (1987) 10767–10776. https://doi.org/10.1029/JC092iC10p10767.

[125] P.T.H.M. Verhallen, L.J.P. Oomen, A.J.J.M. v. d. Elsen, J. Kruger, J.M.H. Fortuin, The diffusion coefficients of helium, hydrogen, oxygen and nitrogen in water determined from the permeability of a stagnant liquid layer in the quasi-s, Chem. Eng. Sci. 39 (1984) 1535–1541. https://doi.org/10.1016/0009-2509(84)80082-2.

[126] W.J. de Blok, J.M.H. Fortuin, Method for determining diffusion coefficients of slightly soluble gases in liquids, Chem. Eng. Sci. 36 (1981) 1687–1694. https://doi.org/10.1016/0009-2509(81)80014-0.

[127] D.L. Wise, G. Houghton, The diffusion coefficients of ten slightly soluble gases in water at 10-60°C, Chem. Eng. Sci. 21 (1966) 999–1010. https://doi.org/10.1016/0009-2509(66)85096-0.

[128] M.H.I. Baird, J.F. Davidson, Annuhr jets-II Gas absorption, Chem. Eng. Sci. 17 (1962) 473–480.

[129] X. Zhao, H. Jin, Correlation for self-diffusion coefficients of H2, CH4, CO, O2 and CO2 in supercritical water from molecular dynamics simulation, Appl. Therm. Eng. 171 (2020). https://doi.org/10.1016/j.applthermaleng.2020.114941.

[130] I.N. Tsimpanogiannis, S. Maity, A.T. Celebi, O.A. Moultos, Engineering Model for Predicting the Intradiffusion Coefficients of Hydrogen and Oxygen in Vapor, Liquid, and Supercritical Water based on Molecular Dynamics Simulations, J. Chem. Eng. Data. 66 (2021) 3226–3244. https://doi.org/10.1021/acs.jced.1c00300.

[131] D.T. Kallikragas, A.Y. Plugatyr, I.M. Svishchev, High temperature diffusion coefficients for O2, H2, and OH in water, and for pure water, J. Chem. Eng. Data. 59 (2014) 1964–1969. https://doi.org/10.1021/je500096r.

[132] I.N. Tsimpanogiannis, O.A. Moultos, L.F.M. Franco, M.B. d. M. Spera, M. Erdős, I.G. Economou, Self-diffusion coefficient of bulk and confined water: a critical review of classical molecular simulation studies, Mol. Simul. 45 (2019) 425–453. https://doi.org/10.1080/08927022.2018.1511903.

[133] M. Laliberté, Model for calculating the viscosity of aqueous solutions, J. Chem. Eng. Data. 52 (2007) 321–335. https://doi.org/10.1021/je0604075.

[134] O.A. Moultos, I.N. Tsimpanogiannis, A.Z. Panagiotopoulos, I.G. Economou, Atomistic molecular dynamics simulations of CO2 diffusivity in H2O for a wide range of temperatures and pressures, J. Phys. Chem. B. 118 (2014) 5532–5541. https://doi.org/10.1021/jp502380r.

[135] A. Al-Yaseri, S. Abdel-Azeim, J. Al-Hamad, Wettability of water-H2-quartz and water-H2-calcite experiment and molecular dynamics simulations: Critical assessment, Int. J. Hydrogen Energy. (2023) in press. https://doi.org/https://doi.org/10.1016/j.ijhydene.2023.05.294.

[136] E.M. Thaysen, I.B. Butler, A. Hassanpouryouzband, D. Freitas, F. Alvarez-Borges, S. Krevor, N. Heinemann, R. Atwood, K. Edlmann, Pore-scale imaging of hydrogen displacement and trapping in porous media, Int. J. Hydrogen Energy. 48 (2023) 3091–3106. https://doi.org/10.1016/j.ijhydene.2022.10.153.

[137] N.S. Muhammed, B. Haq, D.A. Al Shehri, Hydrogen storage in depleted gas reservoirs using nitrogen cushion gas: A contact angle and surface tension study, Int. J. Hydrogen Energy. (2023). https://doi.org/10.1016/j.ijhydene.2023.06.208.

[138] N.S. Muhammed, B. Haq, D. Al Shehri, Role of methane as a cushion gas for hydrogen storage in depleted gas reservoirs, Int. J. Hydrogen Energy. (2023). https://doi.org/10.1016/j.ijhydene.2023.04.173.